Archive of Applied Mechanics (2026) 96:47
https://doi.org/10.1007/s00419-026-03033-4

ORIGINAL

Ahmed Mohammad Wasfi Alhasan · Ahmad Reshad Noori

Free vibration analysis of functionally graded nanobeams via complementary functions method in the laplace domain

Received: 19 October 2025 / Accepted: 7 January 2026 / Published online: 12 February 2026

Abstract This study presents a unified framework for the free vibration analysis of functionally graded (FG) nanobeams within Eringen's nonlocal elasticity, consistently formulated under Euler–Bernoulli (EBT) and Timoshenko (TBT) beam theories. The canonical first-order governing equations are derived in a unified closed-form manner and solved using the Complementary Functions Method (CFM) in the Laplace domain. A comprehensive parametric study addresses four boundary conditions with variations in slenderness ratios, gradation indices, and nonlocal parameters. The primary contribution of this work lies in providing a unified closed-form canonical state-space formulation for nonlocal FG nanobeams under both EBT and TBT, and in demonstrating that the Laplace–CFM implementation offers a stable and efficient eigen-solver with consistent boundary enforcement across multiple support conditions. The resulting benchmark frequencies can serve as a reliable reference for verifying of future refined or multi-physics nanobeam models. The results confirm monotonic frequency softening with increasing nonlocal parameter and with grading toward the softer constituent. The EBT–TBT discrepancy is most pronounced for low-slenderness ratios, highlighting the role of shear deformation and rotary inertia in short/thick nanobeams, while the two theories converge as slenderness increases.

Keywords Functionally Graded Nanobeams · Nonlocal Elasticity · Beam Theories · Complementary Functions Method · Free vibration Analysis

1 Introduction

Nonlocal elasticity enabled scale-aware beam models that correct classical over-stiffness at nanometric lengths. Eringen's [1] introduced an intrinsic material length that produces frequency softening; Peddieson et al. [2] initiated beam applications; and Reddy [3] established unified nonlocal beam/plate equations, foundational for vibration modeling. Within this framework, FG beams with through-thickness stiffness and density variation enable resonance tuning in NEMS/MEMS. Under the EBT, Nazemnezhad and Hosseini-Hashemi [5] reported broad datasets showing two robust trends: larger nonlocal length scales reduce nondimensional frequencies, and shifting gradation toward the softer constituent lowers them further. Finite-element EBT models by Esen et al. [6] corroborated these patterns across various supports and slenderness ratios. Moving beyond EBT, higher-order shear-deformation models by Ebrahimi and Barati [7] captured shear and rotary inertia, predicting slightly lower frequencies that approach EBT as slenderness increases.

A. M. W. Alhasan (✉) · A. R. Noori
Department of Civil Engineering, Istanbul Gelisim University, Istanbul, Türkiye
e-mail: ahmed.ahmed4@ogr.gelisim.edu.tr

A. R. Noori
e-mail: arnoori@gelisim.edu.tr

Alongside FEM, compact spectral and series-type strategies are widely used for eigenproblems. The Differential Quadrature Method (DQM) of Pradhan and Murmu [8] achieves high accuracy with few nodes for nonlocal beams. Şimşek [9] extended these approaches to FG nanobeams and higher modes, and the early nanobeam DQM study of Akgöz and Civalek [10] established consistency with classical benchmarks. Refined nonlocal shear theories by Thai and Vo [11] and by Thai and Choi [12] eliminate ad-hoc shear-correction factors, while the review by Sayyad and Ghugal [13] provides a critical appraisal of bending, buckling, and vibration models for laminated and sandwich beams.

To capture additional length-scale effects beyond Eringen's stress-type nonlocality, nonlocal strain-gradient frameworks were developed. Tang and Qing [14] derived analytical Timoshenko solutions and highlighted the competition between nonlocal softening and gradient hardening. Aifantis [15] showed that gradient hardening significantly influences free-vibration spectra. Reddy and Pang [16] developed nonlocal beam models for carbon nanotubes and identified size-effect regimes relevant to the hardening–softening competition in vibration. Geometry also matters: Hosseini and Rahmani [17] showed curved FG nanobeams under nonlocal TBT retain the trend of decreasing frequencies with increasing nonlocal length, whereas Huynh et al. [18] used an isogeometric approach to show that increasing curvature elevates natural frequencies via geometric stiffness. Gurtin and Murdoch [19] provided the surface-elasticity framework; Hosseini-Hashemi et al. [20] and Trabelssi et al. [21] showed surface and neutral-axis effects shift absolute frequencies while preserving primary sensitivities to nonlocal length, gradation, and slenderness. Energy-based formulations remain useful for S–S baselines and code checks, as noted by Pavić [22]. For general boundary conditions and variable coefficients, FEM is the workhorse; Ganapathi et al. [23] developed a nonlocal higher-order shear-deformation FEM for curved FG nanobeams and reported free-vibration spectra across supports and curvatures suitable for benchmark comparisons. DQM by Ghadiri and Shafiei [24] attains near-FEM accuracy with far fewer degrees of freedom, enabling rapid parametric sweeps. Symplectic formulations by Leung and Mao [25] provided structure-preserving eigen-solvers. The Dynamic Stiffness Method by Su and Banerjee [26] achieved machine-precision eigenvalues for piecewise-uniform segments and was extended to nonlocal members by Taima et al. [27]. Recently, the CFM frameworks by Celebi et al. [28], Yildirim [29], and Noori et al. [30] for graded structures assemble fundamental solutions and enforce boundary determinants to treat variable-coefficient operators efficiently in free vibration.

Recent nonlocal/meshless formulations, including RBF discretization's by Hosseini et al. [31], efficient nonlocal strain-gradient models in thermal fields by Merzouki and Houari [32], and FG nanobeam studies across boundary conditions by Ehyaei et al. [33], deliver high-fidelity free-vibration spectra when nonlocal operators are treated carefully. Metallic FGM S–S results under nonlocal FSDBT by Loja et al. [34] enable checks on grading direction and nondimensionalization. Ebrahimi and Salari [35] and Ghadiri and Jafari [36] showed that thermal fields and tip masses reduce natural frequencies yet preserve additive nonlocal softening. Ebrahimi and Salari [37] showed that temperature-dependent FG properties drift frequencies in size-dependent Timoshenko FG nanobeams without altering sensitivities to the nonlocal parameter and material gradation. Şimşek and Yurtcu [38] provided analytical nonlocal Timoshenko solutions confirming persistent nonlocal softening and diminishing shear influence with increasing slenderness. Hosseini-Hashemi et al. [39] reproduced analogous electromechanical patterns in graded piezoelectric nanobeams. Wang et al. [40] provided classic nonlocal Timoshenko baselines central for mode-ordering checks. Hosseini et al. [41] showed that porosity chiefly lowers frequencies while leaving dominant sensitivities to nonlocal length and gradation intact.

The framework builds on classical elasticity by Landau et al. [42] and on the nonlocal continuum field theory by Eringen and Wegner [43], enabling consistent one-dimensional beam reductions for free vibration. Wang and Varadan [44] confirmed nonlocal resonance fidelity, motivating resonance-centric nanobeam models. Shear and rotary effects are included via Timoshenko's shear correction, indicating when TBT should replace EBT [45]. For functional grading, Sankar [46] obtained integrals for the Eigen problem through-thickness laws and the section. Aydogdu [47] connected Eringen's constitutive idea to practical one-dimensional members and provided a specialized nonlocal EBT for FG beams with implementable parameterizations. Nazmul et al. [48] presented analytical free-vibration solutions for bi-directional FG nanobeams within a nonlocal Euler–Bernoulli framework and supplied closed-form benchmarks for gradation and size effects. Bensaid [49] proposed a refined nonlocal hyperbolic shear-deformation beam model that reduces reliance on ad-hoc shear-correction factors and yields accurate eigenfrequency predictions for nanoscale beams. Thai [50] developed a general nonlocal beam theory for bending, buckling, and vibration that serves as a compact baseline for comparison. Noori et al. [51] showed that the CFM yields a stable state-space formulation for FG beams with straightforward determinant-based boundary enforcement, while Thai et al. [52] clarified where gradient hardening can offset nonlocal softening. Alshorbagy et al. [53] supplied mesh-based verification consistent with these modeling choices. Extensions relevant to graded nanobeams include tapered members with surface energy, where Shanab and Attia [54] emphasized the influence of neutral-axis placement and surface terms on absolute frequencies without altering the core nonlocal and gradation trends.

Beyond single members, CFM analyses of graded porous frames by Rasooli et al. [55] demonstrate robustness for variable-coefficient operators, and the graded sandwich-plate study by Noori [56] confirms portability to other graded continua. For spectral discretization, GDQ studies such as Fereidoon et al. [57] guide node placement and convergence, while bi-directional FG nanobeam spectra by Nejad and Hadi [58] provide external benchmarks. Comparative nonlocal EBT–TBT solutions by Uymaz [59] isolate shear/rotary effects from pure nonlocal softening. The nonlocal strain-gradient mechanics of Li and Hu [60] frame the interplay between stress-type softening and gradient-induced hardening. Li [61] offers a unified EBT/TBT treatment ensuring consistent operators and nondimensional frequencies across slenderness and gradation. Calim [62, 63] examined the free vibration of beams resting on elastic foundations. Mirafzal and Fereidoon [64] showed that viscoelasticity and temperature dependence further depress natural frequencies, even under magnetic loading. [65] introduced a unified nonlocal plus surface-energy framework explaining how surface elasticity adjusts spectra while preserving the primacy of nonlocal length scale, gradation, and slenderness.

Related microscale beam studies include Akgöz and Civalek [9], who performed MCST/Rayleigh–Ritz free-vibration analysis of AFG tapered Euler–Bernoulli microbeams, and Akgöz and Civalek [66], who provided benchmark axial-buckling solutions via strain-gradient elasticity/MCST with variational boundary conditions. Civalek and Demir [67] developed a nonlocal Euler–Bernoulli microtubule model solved by DQM, showing Eringen-parameter softening across loads and boundaries. Akgöz and Civalek [68] presented a higher-order strain-gradient shear-deformation beam with a closed-form solution for the bending/vibration. Jalaei and Civalek [69] mapped dynamic-instability regions for viscoelastic porous FG nanobeams on a visco-Pasternak foundation under axial/magnetic excitation. In related kinematics, Tounsi et al. [70] introduced a four-unknown RTSDT for thermoelastic FGM sandwich plates with parabolic through-thickness shear and no correction, while Bourada et al. [71] proposed a three-unknown higher-order FG beam theory. Size-dependent FG microbeams were analyzed by Al-Basyouni et al. [72] using a unified MCST with variable length scale. Micro-beams were analyzed by Alimirzaei et al. [73] via MSGT-FEM and by Belabed et al. [74] through a hyperbolic five-unknown shear–normal plate theory. Additionally, Aria and Friswell [75] developed a nonlocal FSDT-FEM for FG nanobeam free vibration and buckling.

The CFM is an effective approach that reduces two-point boundary-value problems to initial-value problems. This method has been widely implemented in the analysis of several engineering problems [75–86]. Recent contributions in 2025 have further enriched the vibration literature on functionally graded structures by addressing advanced modeling aspects, broader parametric and boundary-condition spaces, and enhanced numerical solution strategies for improved accuracy and efficiency [87]. Other recent studies have also emphasized the importance of stable and efficient frameworks for handling graded material distributions and size-dependent effects in complex structural settings [88]. In addition, large-scale investigations within contemporary structural-mechanics platforms continue to demonstrate the growing interest in refined formulations and robust computational tools for FG systems [89]. These ongoing developments reinforce the relevance of unified approaches for nonlocal-FG beam vibration, which the present study complements through a consistent EBT/TBT canonical formulation and a Laplace-domain CFM solution supported by comprehensive benchmark datasets [4].

This paper is related to our broader research interest in CFM-based analysis of graded structural members. However, the present study is distinct in that it develops a unified Eringen-based nonlocal free-vibration formulation for FG nanobeams under both EBT and TBT, derives the canonical closed-form first-order equations, and implements a Laplace-domain CFM eigen-solution to generate extensive, cross-validated benchmark frequency sets across multiple boundary conditions and slenderness ranges. The above survey shows that canonical equations of the free-vibration behavior of nano FG beams have not been reported yet in the available literature. The present work is limited to linear free vibration to establish a unified and validated canonical formulation for FG nanobeams under Eringen's nonlocal elasticity within both EBT and TBT. Incorporating geometric nonlinearity would lead to amplitude-dependent frequency relations and modified operators that require a dedicated formulation and solution strategy, which is beyond the scope of the current article and will be addressed in future studies.

The novelties of this paper are as follows: The governing equations of the problem at hand are obtained and solved numerically via the CFM in the Laplace space for the first time. The presented equations for the free-vibration analysis of FG nanobeams rigorously account for the size-dependent (nonlocal) effects and power-law material gradation under Euler–Bernoulli and Timoshenko kinematics. Similarly, thermal fields

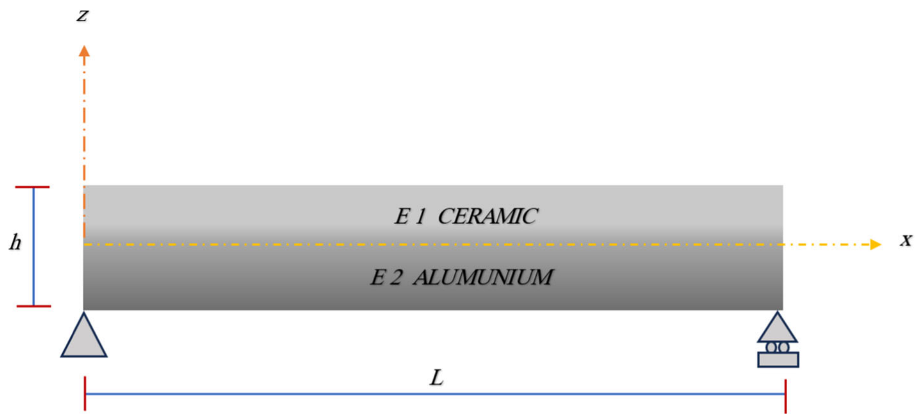

Fig. 1 Simply supported FG nano beam

and temperature-dependent material properties are not considered here to isolate the coupled influence of nonlocality, functional grading, slenderness, and boundary conditions on the free-vibration spectrum. The current results, therefore, provide a clean benchmark baseline for subsequent thermo-nonlocal FG nanobeam formulations. The approach extends CFM to nonlocal eigenproblems and provides reproducible benchmark frequency sets for verification.

The present framework is formulated to cover a broad spectrum of structural-mechanics applications, including bending, stability, and dynamic response. For time-invariant cases such as static bending and classical buckling, the CFM can be applied directly without the need for a Laplace-domain treatment. In contrast, for the time-dependent vibration of heterogeneous Nano FG beams, the Laplace transformation is employed to remove the explicit time dependence and to obtain a canonical ODE system compatible with CFM. The canonical equations of motion derived in the present study thus form the methodological backbone of the proposed approach and constitute one of its main contributions. To clarify the contribution with respect to the extensive nonlocal-FG literature, the present study is positioned primarily as a unified formulation and benchmark-oriented work rather than a new constitutive theory. The main advances are threefold: (i) a consistent closed-form canonical first-order state-space system for Eringen-type nonlocal FG nanobeams under both EBT and TBT, derived within a single framework; (ii) a Laplace-domain CFM eigen-solution that converts the original two-point boundary-value eigenproblem into a numerically stable initial-value setting with determinant-based boundary enforcement, enabling efficient multi-BC computations; and (iii) a systematic, cross-validated benchmark dataset spanning slenderness, gradation, and nonlocality that can be directly used for verification of alternative nonlocal and higher-order beam formulations. These contributions are intended to provide a reliable reference platform and a reusable solver structure for subsequent extensions to smart or multi-physics nanobeam systems.

2 Materials and method

The Complementary Functions Method (CFM) is adopted because it provides a stable and efficient route for solving two-point boundary-value eigen problems with variable coefficients and multiple boundary conditions. By constructing linearly independent complementary solutions and enforcing boundary conditions through a determinant-based formulation, CFM reduces the original eigenproblem to a numerically robust initial-value framework. This feature is particularly advantageous for extensive parametric studies in nonlocal FG nanobeams where repeated solutions across slenderness, grading, and boundary configurations are required.

In this section, the free-vibration response of (FG) nanobeams is examined by separately applying TBT and EBT beam theories.

Consider an FG nano beam given in Fig. 1 with height of h, Length of L, and width of b.

Timoshenko beam theory is included to account for transverse shear deformation and rotary inertia, which can significantly influence the free-vibration spectrum of short and thick FG nanobeams. Using both EBT and TBT enables a consistent quantification of shear-related effects at low-slenderness ratios and demonstrates the expected convergence of the two theories as slenderness increases. The elastic modulus is modeled as a continuously differentiable function of the thickness coordinate z, constructed by a power-law mixture that smoothly bridges the properties of two constituent materials, for any property $P(z) \in \{E,\ G,\ \rho\}$, the standard power-law description reads

$$P(z) = P_1 + (P_2 - P_1)\left(\frac{z + \frac{h}{2}}{h}\right)^k \tag{1}$$

this functional grading produces a monotonic profile $P(z)$ transitioning from the softer to the stiffer phase according to the chosen exponent, and it can be written as follows:

$$E(z) = E_2 + (E_1 - E_2)\left(\frac{z + \frac{h}{2}}{h}\right)^k \tag{2}$$

$$\rho(z) = \rho_1 + (\rho_2 - \rho_1)\left(\frac{z + \frac{h}{2}}{h}\right)^k, \tag{3}$$

where E_1 and E_2 are the moduli at the bottom and top surfaces, h is the thickness, and $k \geq 0$ is the gradation index controlling the transition rate. This spatial variation tunes the frequency spectrum by redistributing stiffness and mass through the depth. Equation (3) prescribes a smooth, monotonic through-thickness density variation via a power-law interpolation between the bottom ρ_1 and top ρ_2 values using the normalized coordinate $\frac{z+\frac{h}{2}}{h}$. The gradation index k shapes the profile: k =1 is linear, k >1 skews toward ρ_1, and 0< k <1 skews toward ρ_2.

The displacement components along the axial (x) and transverse (z) directions are denoted by $u_x(x,\ z,\ t)$ and $u_z(x,\ z,\ t)$, with $u(x,\ t)$ the mid-axis axial displacement, $w(x,\ t)$ the transverse deflection, and $\Theta(x,\ t)$ the cross-section rotation

and for TBT theory, axial displacement includes the rotation of the cross-section

$$U_x = u(x,t) + z \cdot \Theta(x,t) \tag{4}$$

$$U_z = w(x,t) \tag{5}$$

Under the small-strain assumption, the linear axial and shear strains follow directly from the TBT displacement field. Using explicit notation for partial derivatives with respect to x,

$$\varepsilon_x = \frac{\partial U_x}{\partial x} = \frac{\partial u}{\partial x} + z\frac{\partial \Theta}{\partial x} \tag{6}$$

$$\gamma_{xz} = \Theta + \frac{\partial w}{\partial x} \tag{7}$$

The material response is taken as linear elastic and locally isotropic at each through-thickness position z. For an FG section, the constitutive moduli vary smoothly with z, so the classical pointwise relations retain their form with z -dependent coefficients:

$$\sigma_x = E(z) \cdot \varepsilon_x \tag{8}$$

$$\tau_{xz} = k_s \cdot G(z) \cdot \gamma_{xz} \tag{9}$$

Equation (8) defines the axial stress from ε_x; in bending, σ_x varies linearly with z and is scaled by the local modulus $E(z)$. Equation (9) gives the transverse shear stress from γ_{xz} with $G(z)$ with ks correcting the nonuniform shear profile (e.g., k_s=5/6 for a rectangle). With constant ν, $G(z)= E(z)/[2(1+\nu)]$, preserving the graded character. These pointwise stresses generate the section resultants via through-thickness integration.

Under linear TBT kinematics, the kinetic energy consists of axial and transverse translational terms, a rotary term, and a coupling term arising from the product of axial and rotational velocities. With the through-thickness density $\rho(z)$,

$$T = \frac{1}{2}\int_0^L \int_A \rho(z)\left[\left(\frac{\partial u}{\partial t}\right)^2 + 2z\left(\frac{\partial u}{\partial t}\right)\left(\frac{\partial \Theta}{\partial t}\right) + z^2\left(\frac{\partial \Theta}{\partial t}\right)^2 + \left(\frac{\partial w}{\partial t}\right)^2\right] dA dx. \tag{10}$$

Introducing the inertia coefficients per unit length I_0, I_1, I_2 (to be defined by through-thickness integrals of $\rho(z)$, $\rho(z)z$, and $\rho(z)z^2$, respectively), the expression condenses to

$$T = \frac{1}{2}\int_0^L \left[I_0\left(\frac{\partial u}{\partial t}\right)^2 + 2I_1\left(\frac{\partial u}{\partial t}\right)\left(\frac{\partial \Theta}{\partial t}\right) + I_2\left(\frac{\partial \Theta}{\partial t}\right)^2 + I_0\left(\frac{\partial w}{\partial t}\right)^2 \right] dx. \tag{11}$$

Here I_0 represents the mass per unit length, I_1 the first mass moment per unit length (capturing axial–rotational coupling), and I_2 the second mass moment per unit length (rotary inertia).

For linear elastic behavior, the strain (potential) energy of the graded TBT beam is expressed in terms of the axial strain u, the curvature Θ, and the engineering shear strain $\gamma_{xz} = \Theta + w_{,x}$. The quadratic form reads

$$\Pi_t = \frac{1}{2}\int_0^L [A_{11}\left(\frac{\partial u}{\partial x}\right)^2 + 2A_{12}\left(\frac{\partial u}{\partial x}\right)\left(\frac{\partial \Theta}{\partial x}\right) + A_{22}\left(\frac{\partial \Theta}{\partial x}\right)^2 + A_{33}(\Theta^2 + 2\Theta\frac{\partial w}{\partial x} + \left(\frac{\partial w}{\partial x}\right)^2]dx. \tag{12}$$

Here A_{11}, A_{12}, A_{22}, and A_{33} are the sectional stiffness coefficients (axial, axial–bending coupling, bending, and shear, respectively), defined by through-thickness integrals in (13)–(19). The last term collects the shear contribution in TBT kinematics via the squared shear strain $(\Theta + w_{,x})^2$.

The sectional coefficients per unit length are defined by through-thickness integration of the graded moduli and density:

$$A_{11} = b\int_{-h/2}^{+h/2} E(z)dz \tag{13}$$

$$A_{12} = b\int_{-\frac{h}{2}}^{+\frac{h}{2}} E(z)\cdot zdz \tag{14}$$

$$A_{22} = b\int_{-\frac{h}{2}}^{+\frac{h}{2}} E(z)\cdot z^2dz \tag{15}$$

$$A_{33} = k_s\cdot b\int_{-\frac{h}{2}}^{+\frac{h}{2}} G(z)dz \tag{16}$$

$$I_0 = b\int_{-\frac{h}{2}}^{+\frac{h}{2}} \rho(z)dz \tag{17}$$

$$I_1 = b\int_{-\frac{h}{2}}^{+\frac{h}{2}} \rho(z)\cdot zdz \tag{18}$$

$$I_2 = b\int_{-\frac{h}{2}}^{+\frac{h}{2}} \rho(z)\cdot z^2dz \tag{19}$$

The axial force, bending moment, and shear force are expressed in terms of the generalized strains $\frac{\partial u}{\partial x}$, $\frac{\partial \Theta}{\partial x}$, and $\frac{\partial w}{\partial x} + \Theta$ through the sectional coefficients defined in (20)–(22):

$$N_x = A_{11}\frac{\partial u}{\partial x} + A_{12}\frac{\partial \Theta}{\partial x} \tag{20}$$

$$M_x = A_{12}\frac{\partial u}{\partial x} + A_{22}\frac{\partial \Theta}{\partial x} \tag{21}$$

$$Q_z = A_{33}(\frac{\partial w}{\partial x} + \Theta) \tag{22}$$

Solving (20) and (21) for the axial and rotational strains gives

$$\frac{\partial u}{\partial x} = \frac{-A_{22}N_x + A_{12}M_x}{A_{12}^2 - A_{11}A_{22}} \tag{23}$$

$$\frac{\partial \Theta}{\partial x} = \frac{A_{12}N_x - A_{11}M_x}{A_{12}^2 - A_{11}A_{22}} \tag{24}$$

The shear relation (22) yields the slope–rotation combination as

$$\frac{\partial w}{\partial x} = \frac{Q_z}{A_{33}} - \Theta \tag{25}$$

For the variational derivation, the Lagrangian functional is taken in quadratic form consistent with the kinetic-energy structure in Eq. (11). Using the generalized velocities $u_{,t}$, $\Theta_{,t}$, and $w_{,t}$, the adopted expression reads

$$\begin{aligned} l = {} & \frac{1}{2}\int_0^L \left[I_0\left(\frac{\partial u}{\partial t}\right)^2 + I_1\left(\frac{\partial u}{\partial t}\right)\left(\frac{\partial \Theta}{\partial t}\right) + I_2\left(\frac{\partial \Theta}{\partial t}\right)^2 + I_0\left(\frac{\partial w}{\partial t}\right)^2 \right] dx \\ & - \frac{1}{2}\int_0^L [A_{11}\left(\frac{\partial u}{\partial x}\right)^2 + 2A_{12}\left(\frac{\partial u}{\partial x}\right)\left(\frac{\partial \Theta}{\partial x}\right) + A_{22}\left(\frac{\partial \Theta}{\partial x}\right)^2 + A_{33}(\Theta^2 + 2\Theta\frac{\partial w}{\partial x} + \left(\frac{\partial w}{\partial x}\right)^2]dx \end{aligned} \tag{26}$$

The one-dimensional balance laws for axial force N_x, shear force Q_z, and bending moment M_x are written in terms of the generalized accelerations $\frac{\partial^2 u}{\partial t^2}, \frac{\partial^2 \Theta}{\partial t^2}$, and $\frac{\partial^2 w}{\partial t^2}$. Denoting N_x, Q_z, and M_x, and using the inertia coefficients from (17–19), the governing relations are

$$\frac{\partial N_x}{\partial x} = I_0\frac{\partial^2 u}{\partial t^2} + I_1\frac{\partial^2 \Theta}{\partial t^2} \tag{27}$$

$$\frac{\partial Q_z}{\partial x} = I_0\frac{\partial^2 w}{\partial t^2} \tag{28}$$

$$\frac{\partial M_x}{\partial x} = I_1\frac{\partial^2 u}{\partial t^2} + I_2\frac{\partial^2 \Theta}{\partial t^2} + Q_z \tag{29}$$

Eringen's differential nonlocal elasticity is accounted for by augmenting the local constitutive–equilibrium structure with scale-dependent terms proportional to the squared nonlocal length parameter μ. In the present setting, this leads to modified kinematic relations that express the axial strain, the transverse slope, and the curvature in terms of the stress resultants and the spatial derivatives of the inertial contributions. Specifically,

$$\frac{\partial u}{\partial x} = \frac{N_x - \mu\frac{\partial}{\partial x}\left(I_0\frac{\partial^2 u}{\partial t^2} + I_1\frac{\partial^2 \Theta}{\partial t^2}\right) - A_{12}\frac{\partial \Theta}{\partial x}}{A_{11}} \tag{30}$$

$$\frac{\partial w}{\partial x} = \frac{Q_z - \mu\frac{\partial}{\partial x}\left(I_0\frac{\partial^2 w}{\partial t^2}\right) - A_{33}\cdot\Theta}{A_{33}} \tag{31}$$

$$\frac{\partial \Theta}{\partial x} = \frac{M_x - \mu\frac{\partial}{\partial x}\left(I_1\frac{\partial^2 u}{\partial t^2} + I_2\frac{\partial^2 \Theta}{\partial t^2} + Q_z\right) - A_{12}\frac{\partial u}{\partial x}}{A_{22}} \tag{32}$$

In Eringen's differential nonlocal elasticity, the intrinsic material length scale is commonly represented by the parameter e_0. In the present work, we therefore define the nonlocal parameter as $\mu = (e_0 a)^2$. To keep the physical discussion aligned with prevailing practice in the nonlocal beam literature, the main parametric interpretation is presented over $\mu = 0-4$. An additional value $\mu = 5$ is included only to demonstrate the numerical robustness of the Laplace–CFM implementation, and no further material-specific physical conclusions are drawn beyond the customary range. The main discussion is restricted to μ =0–4, while $\mu = 5$ is reported only to demonstrate the numerical robustness of the Laplace–CFM solver.

Parameter μ encapsulates the intrinsic material length and is dimensionless if normalized by the beam length. The additional μ-scaled terms introduce higher-order spatial dependence through the derivatives of the inertia-based combinations, thereby capturing size effects in the axial, shear, and bending responses.

The unilateral Laplace transform in time is defined by:

$$L\{f(t)\} = F(s) = \int_0^\infty e^{-st} f(t)dt \tag{33}$$

For time derivatives:

$$L\{f_{,t}\} = sF - f(0), L\{f_{,tt}\} = s^2F - sf(0) - f^{\dot{}}(0) \tag{34}$$

The transform commutes with spatial differentiation, so that

$$L\left\{\frac{\partial}{\partial x}F(x,t)\right\}=\frac{d}{dx}\underline{f}(x,s) \tag{35}$$

With overbars denoting Laplace images,

$$\underline{U}(x,s)=L\{u\},\underline{W}(x,s)=L\{w\},\underline{\Theta}(x,s)=L\{\theta\} \tag{36}$$

Using Eqs.(34) to replace $(\cdot)_{,x} by \overline{(\cdot)}_{,x}$, the first-order relations in the s-domain take the form, and the canonical equation for TBT beam is obtained as follows:

$$\frac{d\underline{u}}{dx}=\frac{-\left(A_{22}+\mu I_2 s^2\right)\underline{N}_x+\left(\left(A_{12}+\mu I_1 s^2\right)\left(\underline{M}_x-\mu I_0 s^2\underline{w}\right)\right)}{-\left(A_{11}+\mu I_0 s^2\right)\left(A_{22}+\mu I_2 s^2\right)+\left(A_{12}+\mu I_1 s^2\right)^2} \tag{37}$$

$$\frac{d\underline{w}}{dx}=\frac{\underline{Q}_z-A_{33}\underline{\Theta}}{A_{33}+\mu I_0 s^2} \tag{38}$$

$$\frac{d\underline{\Theta}}{dx}=\frac{-\left(\left(A_{11}+\mu I_0 s^2\right)(M_x-\mu I_0 s^2\underline{w})\right)+\left(A_{12}+\mu I_1 s^2\right)\underline{N}_x}{-\left(A_{11}+\mu I_0 s^2\right)\left(A_{22}+\mu I_2 s^2\right)+\left(A_{12}+\mu I_1 s^2\right)^2} \tag{39}$$

$$\frac{d\underline{N}_x}{dx}=I_0 s^2\underline{u}+I_1 s^2\underline{\Theta} \tag{40}$$

$$\frac{d\underline{Q}_z}{dx}=I_0 s^2\underline{w} \tag{41}$$

$$\frac{d\underline{M}_x}{dx}=I_1 s^2\underline{u}+I_2 s^2\underline{\Theta}+\underline{Q}_z \tag{42}$$

Here

$$\underline{u}\,(x,\,s)=\mathcal{L}\left\{u\,(x,\,t)\right\},\ \underline{w}\,(x,\,s)=\mathcal{L}\left\{w\,(x,\,t)\right\},\ \underline{\Theta}\,(x,\,s)=\mathcal{L}\left\{\Theta\,(x,\,t)\right\},\ \underline{N}_x=L\left\{N_x\right\}$$

$\underline{Q}_z=L\{Q_z\}$, and $\underline{M}_x=L\{M_x\}$ denote the Laplace images of the axial force, shear force, and bending moment, respectively. The CFM is adopted to derive numerical solutions for the free-vibration of (FG) nanobeams described by the nonlocal EBT and TBT theories.

In the Laplace-domain first-order system, the second relation governs transverse kinematics. For TBT, the shear-constitutive is $\frac{dw}{dx}=\frac{\underline{Q}_z-A_{33}\Theta}{A_{33}+\mu I_0 s^2}$ which couples $\underline{w}$ and Θ via the shear stiffness A_{33}. In EBT, transverse shear is suppressed ($\gamma_{xz}=0$) enforcing $\underline{\Theta}=-\underline{w}_{,x}$; therefore, the second equation collapses to the purely kinematic identity $\frac{dw}{dx}=-\underline{\Theta}$, no A_{33} or $\underline{Q}_z$ terms appear. The axial/rotational derivative formulas remain unchanged and use the same determinant $\Delta(s)=(A_{11}+\mu I_0 s^2)(A_{22}+\mu I_2 s^2)-(A_{12}+\mu I_1 s^2)^2$ in both TBT and EBT. So, the canonical equation for EBT beam is obtained as follows:

$$\frac{d\underline{u}}{dx}=\frac{-\left(A_{22}+\mu I_2 s^2\right)\underline{N}_x+\left(\left(A_{12}+\mu I_1 s^2\right)\left(\underline{M}_x-\mu I_0 s^2\underline{w}\right)\right)}{-\left(A_{11}+\mu I_0 s^2\right)\left(A_{22}+\mu I_2 s^2\right)+\left(A_{12}+\mu I_1 s^2\right)^2} \tag{43}$$

$$\frac{d\underline{w}}{dx}=-\underline{\Theta} \tag{44}$$

$$\frac{d\underline{\Theta}}{dx}=\frac{-\left(\left(A_{11}+\mu I_0 s^2\right)(\underline{M}_x-\mu I_0 s^2\underline{w})\right)+\left(A_{12}+\mu I_1 s^2\right)\underline{N}_x}{-\left(A_{11}+\mu I_0 s^2\right)\left(A_{22}+\mu I_2 s^2\right)+\left(A_{12}+\mu I_1 s^2\right)^2} \tag{45}$$

$$\frac{d\underline{N}_x}{dx}=I_0 s^2\underline{u}+I_1 s^2\underline{\Theta} \tag{46}$$

$$\frac{d\underline{Q}_z}{dx}=I_0 s^2\underline{w} \tag{47}$$

$$\frac{d\underline{M}_x}{dx}=I_1 s^2\underline{u}+I_2 s^2\underline{\Theta}+\underline{Q}_z \tag{48}$$

In the canonical equations, s is the Laplace parameter. Free vibration is recovered by setting $s = i\omega$. Due to its reliability and precision, the CFM has been adopted to solve the first-order state-space form of the FG nanobeam under Eringen's nonlocal elasticity.

$$\{\mathbf{F}\} + [\mathbf{W}(s)]\{\mathbf{Y}\} = \{\mathbf{Y}\}\prime \tag{49}$$

$$\{\mathbf{Y}\} = \begin{bmatrix} u & w & \varphi & N_x & Q_z & M_x \end{bmatrix}^{\mathrm{T}} \tag{50}$$

$$[\mathbf{W}(s)] = \begin{bmatrix} 0 & \gamma_{12}(s,x) & 0 & \gamma_{14}(s,x) & 0 & \gamma_{16}(s,x) \\ 0 & 0 & \gamma_{23}(s,x) & 0 & \gamma_{25}(s,x) & 0 \\ 0 & \gamma_{32}(s,x) & 0 & \gamma_{34}(s,x) & 0 & \gamma_{36}(s,x) \\ s^2 I_0 & 0 & s^2 I_1 s & 0 & 0 & 0 \\ 0 & s^2 I_0 & 0 & 0 & 0s & 0 \\ s^2 I_1 & 0 & s^2 I_2 & 0 & 1 & 0 \end{bmatrix} \tag{51}$$

$$\{\mathbf{F}\} = \begin{bmatrix} 0 \\ 0 \\ 0 \\ -p_x(s,x) \\ -p_z(s,x) \\ 0 \end{bmatrix}, \tag{52}$$

where $\{\mathbf{Y}\}$ is the state vector, $[\mathbf{W}(s)]$ is the differential transfer matrix, and $\{\mathbf{F}\}$ is the load vector.

For free vibration, there are no external loads; i.e.,

$$p_x(x) = p_z(x) = 0 \Rightarrow \{\mathbf{F}\} = 0 \tag{53}$$

$$\alpha_{11} = A_{11} + \mu I_0 s^2 \tag{54}$$

$$\alpha_{12} = A_{12} + \mu I_1 s^2 \tag{55}$$

$$\alpha_{22} = A_{22} + \mu I_2 s^2 \tag{56}$$

$$\alpha_{33} = A_{33} + \mu I_0 s^2 \tag{57}$$

$$\Delta_s = \alpha_{11}\alpha_{22} - \alpha_{12}^2 \tag{58}$$

$$\gamma_{12}(s,x) = \frac{\alpha_{12}\mu I_0 s^2}{\Delta_s} \tag{59}$$

$$\gamma_{14}(s,x) = \frac{\alpha_{22}}{\Delta_s} \tag{60}$$

$$\gamma_{16}(s,x) = -\frac{\alpha_{12}}{\Delta_s} \tag{61}$$

$$\gamma_{23}(s,x) = -\frac{A_{33}}{\alpha_{33}} \tag{62}$$

$$\gamma_{25}(s,x) = \frac{1}{\alpha_{33}} \tag{63}$$

$$\gamma_{32}(s,x) = -\frac{\alpha_{11}\mu I_0 s^2}{\Delta_s} \tag{64}$$

$$\gamma_{34}(s,x) = -\frac{\alpha_{12}}{\Delta_s} \tag{65}$$

$$\gamma_{36}(s,x) = \frac{\alpha_{11}}{\Delta_s} \tag{66}$$

The CFM constructs six linearly independent complementary functions (fundamental solutions) $U^{(m)}(x, s)$ by solving (49) with unit initial vectors. The general solution in each element is

$$\{\mathbf{Y}(x,s)\} = \sum_{m=1}^{6} C_m \{U^{(m)}(x,s)\} \tag{67}$$

The constants C_m are obtained from the mechanical boundary conditions at $x = 0,\ L$. Substituting (67) into the boundary equations yields a homogeneous algebraic system

$$B(s)C = 0 \tag{68}$$

$$C = [C_1, \ldots, C_6]^{\mathrm{T}} \tag{69}$$

which has non-trivial solutions only if

$$\det B(s) = 0 \tag{70}$$

The use of the Laplace domain in conjunction with the CFM is not introduced merely as an alternative route to compute eigenfrequencies. Rather, it provides a uniform state-space representatiosn in which the time dependence is systematically eliminated and the governing relations for EBT and TBT can be written in a single canonical first-order structure with a consistent determinant-based boundary operator. This uniformity is particularly useful for nonlocal FG systems with multiple boundary conditions and repeated parametric evaluations, where numerical stability and reproducibility of the eigen-determinant evaluation become critical.

Setting $s = i\omega$ gives the frequency equation; the natural circular frequencies ω_n are the roots of det[B $(i\omega)] = 0$. The associated mode shapes follow from (69) with the corresponding eigenvector C and can be normalized as needed.

The table below summarizes the boundary conditions for FG nanobeams under different support configurations (*C–C, C–S, S–S, and C–Free*). Each case specifies the displacement, rotation, and force/moment constraints at both ends, which are essential for formulating and solving the governing equations.

The present boundary conditions are implemented in the same mechanical form adopted by widely used differential nonlocal beam benchmarks; the excellent agreement with multiple established references indicates that the adopted boundary enforcement is consistent for the current eigenproblem setting. The roots ω_n are the natural circular frequencies. Each mode is normalized so $0 \le x \le L|w_n(x)| = 1$, and the frequencies are reported in dimensionless form:

$$\underline{\omega_n} = \frac{\omega_n L^2}{h}\sqrt{\frac{\rho_0}{E_0}} \tag{71}$$

After constructing the CFM solution, a matrix is formulated M and the problem is solved using standard numerical algorithms, and the resulting frequencies and mode shapes are validated against benchmark solutions. This formulation forms as Fortran code used in this study for free-vibration analysis of FG nanobeams.

3 Numerical results and discussion

Free vibration is treated as a variable-coefficient eigenvalue problem and solved using the complementary functions method (CFM). The FG configuration follows Fig. 1, with ceramic at the top face and aluminum at the bottom. Face properties used throughout are ceramic ($E_1 = 380$GPa, $\rho_1 = 3960 kg/\mathrm{m}^3$) and aluminum ($E_2 =$ 70GPa, $\rho_2 = 2702 kg/\mathrm{m}^3$). The through-thickness fields $E(z)$ and $\rho(z)$ obey the same power-law gradation; Poisson's ratio is fixed at $\nu = 0.30$, hence $G(z) = E(z)/[2(1+\nu)]$. For Timoshenko kinematics, we adopt the shear-correction $k_s = 5/6$. Geometry is normalized with $b = 1$ and $h = 1$ (with L/h varied where indicated), and natural frequencies are reported in nondimensional form.

The nonlocal parameter μ is examined primarily within the commonly adopted range $\mu = 0 - 4$ in the main discussion. Similarly to [47] and [75], an additional value $\mu = 5$ is included as an extended sensitivity and numerical robustness check for the Laplace–CFM framework. The main trends and conclusions remain unchanged within $\mu \le 4$. The slenderness ratio *L/h* is varied by changing the beam length L while keeping h constant. In the present parametric framework, the dimensionless nonlocal parameter μ is treated as an independent control variable to decouple the influence of slenderness from nonlocality. For a specific material with a fixed intrinsic length, μ would scale inversely with *L*.

To embed the effect of functional gradation in the computations, the sectional stiffness coefficients A_{11}, A_{12}, A_{22}, and A_{33} (axial, axial–bending coupling, bending, and shear stiffness, respectively) were evaluated analytically for each gradation index k. Using the power-law profiles $E(z)$ and $G(z)$ defined, the closed-form expressions of the integrals were derived for the representative cases $k = \{1,3,10\}$. These expressions were then embedded directly in the Fortran implementation to assemble the elementwise constant stiffness blocks used by the CFM state-space solver. For consistency of the eigenproblem, the inertia coefficients I_0, I_1, and I_2 were computed from the corresponding closed-form integrals of $\rho(z)$. The resulting A_{ij} and I_i coefficients feed both the EBT and TBT formulations uniformly, ensuring that the reported natural frequencies reflect the combined influence of gradation and nonlocality without numerical quadrature errors in the section integrals.

Table 2 presents first-mode nondimensional frequencies of an isotropic simply supported nanobeam with $L/h = 10$, evaluated for increasing nonlocal parameter μ. Results from the present CFM model are benchmarked against EBT and TBT. Frequencies consistently decrease with μ, indicating nonlocal softening (about 15% reduction from μ =0 to 4).

Table 3 reports nondimensional natural frequencies of an isotropic supported nanobeam at L/h = 10,20,50 as the nonlocal parameter μ increases from 0 to 4. Results include Ref [47] EBT (1st mode), TBT (1st/2nd modes), and the present CFM–TBT (1st/2nd modes). Frequencies decrease steadily withμ, reflecting nonlocal softening. The EBT–TBT difference in the first mode narrows with increasing slenderness and vanishes by L/h = 50 (e.g., at μ =0, 9.8696 vs. 9.8645). As shown, the present CFM very closely matches with Ref [47], with deviations of only 0.1–0.8%, while the μ =0 EBT baseline ≈π2 validates normalization.

Table 4 presents nondimensional first-mode frequencies of a very slender simply supported nanobeam (L/h = 100) as the nonlocal parameter μ increases from 0 to 5 in steps of 0.5. Across all models Reddy's EBT, FSDBT, RBT, LBT, Aria's FSDBT, and the present CFM—the results are nearly identical, with differences ≤ (10 − 2%), confirming that shear and rotary effects are negligible at this slenderness. Frequencies decrease monotonically with μ, dropping about 18% from π2 = 9.8696 at μ =0 to ≈8.0747 at μ =5. This trend verifies the expected nonlocal softening and demonstrates both the correctness of normalization and the robustness of the proposed solver.

Table 5 reports first-mode nondimensional frequencies of a simply supported FG nanobeam with L/h = 20 for nonlocal parameters μ =0–5 and gradation indices k =0, 1, ∞. Present CFM results align very closely with those of Aria across all cases, confirming proper normalization and numerical accuracy. The results highlight two consistent trends: frequencies decrease with increasing μ due to nonlocal softening and shift further downward as the material composition moves toward the softer constituent (k:0 → 1 → ∞). Mode ordering and smooth parameter variation remain fully preserved.

Table 6 presents first-mode nondimensional frequencies of a clamped–simply supported FG nanobeam with L/h = 20 for nonlocal parameters ($\mu = 0 - 5$)and gradation indices k =0, 1, ∞. Results from Aria and the present CFM are in near-perfect agreement, confirming the consistency of the formulation. Frequencies decrease steadily with increasing μ, while the gradation ordering is preserved at all values (k =0 highest, k = 1 intermediate, k =∞ lowest). The dataset exhibits smooth, well-behaved trends without anomalies.

Table 7 shows first-mode nondimensional frequencies of a clamped–clamped FG nanobeam with $L/h = 20$ as the nonlocal parameter μ from 0 to 5 varies for gradation indices k =0, 1, ∞. Present CFM results reproduce Aria's values almost exactly across all cases. As with other boundary conditions, frequencies decrease uniformly with increasing μ, while higher gradation toward the softer constituent consistently lowers them further. The trends remain smooth and well ordered, providing a reliable benchmark for the most constrained support configuration.

Table 8 presents first-mode nondimensional frequencies of a simply supported FG nanobeam with L/h = 100L for μ =0 − 5 and k =0,1,∞. Present CFM values match with those Ref [75]. essentially entry-by-entry, confirming that shear/rotary effects are negligible at this slenderness. Frequencies decrease monotonically with μ (nonlocal softening), and the gradation ordering is preserved for all μ (k =0 highest → k = 1 → k = ∞ lowest). Trends are smooth and free of anomalies.

Table 9 presents first-mode nondimensional frequencies of a clamped–simply supported FG nanobeam with L/h = 100 for μ =0 − 5 and k =0,1,∞. Present CFM values closely match with those of Ref [75]. across all cases; only a small, uniform offset appears for k =1 as μ varies, plausibly due to minor modeling-convention differences (e.g., shear-correction factor or neutral-axis placement). Frequencies decrease monotonically with μ, and for any fixed μ, the expected gradation ordering persists (k =0 highest → k = 1 → k = ∞ lowest), with smooth, anomaly-free trends.

Table 10 presents first-mode nondimensional frequencies of a clamped–clamped FG nanobeam with L/h = 100L for μ =0 − 5 and k =0,1,∞. Present CFM values match with those of Ref [75]. essentially entry-by-entry. As the most constrained case, absolute frequencies are the highest among the three BCs, yet the same trends hold: increasing μ yields uniform nonlocal softening, and shifting the gradation toward the softer constituent lowers the frequency at every μ. The results are smooth and consistently ordered.

Table 11 presents first-mode nondimensional frequencies of a S–S FG nanobeam with $L/h = 10$ over μ =0 − 5 and $k \in \{0,1,3,5,10,\infty\}$. Frequencies decrease monotonically with μ (nonlocal softening), and at any fixed μ

Table 1 The boundary conditions for FG nanobeams under different support configurations

Configuration	Conditions at $x = 0$	Conditions at $x = L$
Fixed–Fixed (C–C)	$u(0) = 0$, $w(0) = 0$,$\Theta(0) = 0$	$u(L) = 0$, $w(L) = 0$, $\Theta(L) = 0$
Fixed–Pinned (C–S)	$u(0) = 0$, $w(0) = 0$, Θ $(0) = 0$,	$u(L) = 0$, $w(L) = 0$, $Mx(L) = 0$
Pinned–Pinned (S–S)	$u(0) = 0$, $w(0) = 0$, $Mx(0) = 0$	$u(L) = 0$, $w(L) = 0$, $M_x(L) = 0$
Cantilever (C–Free)	$u(0) = 0$, $w(0) = 0$,$\Theta(0) = 0$	$N_x(L) = 0$,$Qz(L) = 0$,$M_x(L) = 0$

Table 2 The nondimensional first-mode frequency of Isotropic S–S nanobeam with those EBT/TBT via present CFM

L/h	μ	k=0	Free vibration analysis			
		EBT Ref [3]	EBT Ref [47]	TBT Ref [47]	EBT Ref [6]	CFM (TBT)
10	0	9.8696	9.8696	9.7443	9.8696	9.70748
	1	9.4159	9.4124	9.2931	9.4159	9.26121
	2	9.0195	9.0133	8.8994	9.0195	8.87132
	3	8.6693	8.6611	8.5517	8.6693	8.52686
	4	8.3569	8.3472	8.2419	8.3569	8.21964

they decline systematically as the gradation shifts toward the softer constituent (k:0 → 1 → 3 → 5 → 10 → ∞). The trends are smooth and consistently ordered across both parameters, providing a reliable short-beam baseline for S–S supports.

Table 12 presents first-mode nondimensional frequencies of a clamped–simply supported FG nanobeam with $L/h = 10$ for μ =0 − 5 and k ∈{0,1,3,5,10,∞}. Frequencies decrease monotonically with μ (nonlocal softening), and for any fixed μ, the gradation ordering persists higher for stiffer compositions (k →0) and lowest at k →∞. Trends are smooth and well-ordered across all parameters, offering a clear reference for this partially restrained boundary condition.

Table 13 presents first-mode nondimensional frequencies of a clamped–clamped FG nanobeam with $L/h =$ 10 for μ =0 − 5 and k ∈{0,1,3,5,10,∞}. As the most constrained case, absolute values are the highest, yet two patterns hold: frequencies decrease monotonically with μ, and at any fixed μ, they drop systematically as the gradation shifts toward the softer constituent (k:0 → ∞). The trends are smooth and well ordered, providing a reliable reference for the fully clamped, low-slenderness configuration.

Table 14 presents the first-mode nondimensional frequencies of a cantilever FG nanobeam at the stated slenderness, spanning $\mu = 0 - 5$ and multiple gradation indices. Frequencies drop with softer grading (at fixed μ) and with increasing μ (at fixed grading). The data are smooth, monotonic, and anomaly-free, providing a reliable cantilever baseline. Synthesis over all tables from 2 to 14 together furnish a unified, cross-validated dataset covering scale (μ), gradation (k), slenderness, and boundary conditions. Isotropic S–S baselines ($k =$ 0; Tables 2 and 3) set the normalization and validate against EBT/TBT and multi-theory references (Reddy, Aydogdu, Aria), recover the classical S–S limit at μ =0, and show EBT–TBT convergence with increasing *L/h*. Full spectra at k =0 for $L/h = 20$ are included. Overall, the CFM–TBT solver delivers smooth parameter dependence, correct mode ordering, and numerical stability, providing a comprehensive reference set (Tables 4, 5, 6, 7, 8, 9, 10, 11, 12, 13 and 14).

Short-beam EBT set ($L/h = 5$). Tables 15, 16, 17, 18, 19, 20, 21, 22, 23, 24, 25 and 26 compile the EBT results for *C–C, C–S, S–S, and C–Free* boundaries, reporting the first three modes over multiple gradation indices. Tables 15, 16, 17, 18, 19, 20, 21, 22 and 23 report the first three EBT modes for *C–C, C–S,* and *S–S,* respectively, while Tables 24–26 give the corresponding cantilever (C–Free) results. A coherent picture emerges: in the supported cases (*C–C/C–S/S–S),* frequencies decrease smoothly and Midmonotonically with the nonlocal parameter μ, and at any fixed μ, they decline systematically as the gradation shifts toward the softer constituent. Absolute levels respect the boundary hierarchy *C–C* > *C–S* > *S–S* > *C–Free*; mode ordering is preserved, with no curve crossings or anomalies. The cantilever set (Tables 24–26) fits cleanly into this map: modes 2–3 follow the same softening-with- μ and soft-grading ordering (with only a minor departure from strict monotonicity at the largest μ in mode 3), whereas the fundamental shows a mild, monotonic increase with μ across gradations—an exception confined to this boundary/mode that does not disturb the overall ordering. Sensitivity to both μ and k grows from the fundamental to higher modes, as expected.

Frequencies fall with larger nonlocality (μ) and softer grading (higher k), and rise with stiffer end constraints; these trends hold even for short beams, where EBT remains smooth and stable, while shear deformation

Table 3 nondimensional first/second TBT frequencies for Isotropic S–S nanobeam under various k vs μ, with those EBT/TBT via present CFM

L/h	μ	k=0	Free vibration analysis			
		EBT 1st Frequency Ref. [47]	TBT 1st Frequency Ref. [47]	TBT 2nd Frequency Ref. [47]	CFM –TBT 1st Frequency	CFM– TBT 2nd Frequency
10	0	9.8696	9.7443	36.8406	9.70748	37.0962
	1	9.4124	9.2931	31.2366	9.26121	31.4105
	2	9.0133	8.8994	27.587	8.87132	27.7303
	3	8.6611	8.5517	24.9727	8.52686	25.0996
	4	8.3472	8.2419	22.9826	8.21964	23.0989
20	0	9.8696	9.8381	38.9645	9.82813	38.82990522
	1	9.7498	9.7187	37.1614	9.70908	37.04482612
	2	9.6343	9.6036	35.5875	9.59425	35.48527213
	3	9.5228	9.4924	34.1979	9.4834	34.10743563
	4	9.415	9.385	32.9594	9.37631	32.87856319
50	0	9.8696	9.8645	39.3976	9.86292	39.37193251
	1	9.8501	9.8451	39.0897	9.84351	39.06469887
	2	9.8308	9.8258	38.789	9.82422	38.764546
	3	9.8117	9.8066	38.4951	9.80503	38.47120775
	4	9.7925	9.7875	38.2078	9.78596	38.18442929

Table 4 Isotropic S–S nanobeam ($k = 0$, $L/h = 100$), nondimensional first-mode frequency vs μ; multi-theory via present CFM

L/h	μ	k=0			Free vibration analysis		
		EBT Ref [3]	FSDBT Ref [3]	RBT Ref [3]	LBT Ref [3]	FSDBT Ref [75]	CFM TBT
100	0	9.8696	9.8683	9.8683	9.8685	9.8679	9.86784
	0.5	9.6347	9.6335	9.6335	9.6337	9.6331	9.63311
	1	9.4159	9.4147	9.4147	9.4149	9.4143	9.41429
	1.5	9.2113	9.2101	9.2101	9.2103	9.2097	9.20973
	2	9.0195	9.0183	9.0183	9.0185	9.018	9.01795
	2.5	8.8392	8.838	8.838	8.8382	8.8377	8.83768
	3	8.6693	8.6682	8.6682	8.6683	8.6678	8.6678
	3.5	8.5088	8.5077	8.5077	8.5079	8.5073	8.50736
	4	8.3569	8.3558	8.3558	8.356	8.3555	8.3555
	4.5	8.2129	8.2118	8.2118	8.212	8.2115	8.2115
	5	8.0761	8.075	8.075	8.0752	8.0747	8.0747

Table 5 (S–S) FG nanobeam, $L\,/\,h = 20$: fundamental nondimensional frequency vs μ for various k comparison with present CFM for TBT

	k=0		k=1		$k=\infty$	
μ	Ref [75]	CFM	Ref [75]	CFM	Ref [75]	CFM
0	5.4603	5.46032	4.2051	4.20369	2.8371	2.83714
1	5.3941	5.39418	4.1541	4.1528	2.8028	2.80277
2	5.3303	5.33038	4.105	4.10372	2.7696	2.76972
3	5.2687	5.2688	4.0576	4.05634	2.7376	2.73762
4	5.2092	5.2093	4.0117	4.01056	2.7067	2.70671
5	5.1517	5.15177	3.9674	3.9663	2.6768	2.67682

mainly shifts magnitudes. To increase frequencies, use smaller k and restrictive supports (especially *C–C*); to decrease them use larger μ, larger k, and less restrictive supports (*C–Free*). Tables 15, 16, 17, 18, 19, 20, 21, 22, 23, 24, 25 and 26 thus serve as reliable, mode-wise benchmarks for verification and resonance tuning.

Mid-slender EBT set ($L/h = 20$). Tables 27, 28, 29, 30, 31, 32, 33, 34, 35, 36, 37 and 38 chart the free-vibration response of FG nanobeams under EBT kinematics across *C–C, C–S, S–S*, and C–Free boundaries for the first three modes and a wide range of gradation indices. For $L/h = 20$, the three-mode EBT datasets are given in Tables 27, 28 and 29 *(C–C)*, 30–32 *(C–S)*, 33–35 *(S–S)*, and 36–38 (C–Free). A consistent pattern emerges: in the supported cases (*C–C/C–S/S–S*), frequencies decline smoothly with the nonlocal parameter μ

Table 6 (C–S) FG nanobeam, $L/h = 20$: fundamental nondimensional frequency vs μ for various k comparison with present CFM for TBT

	k=0		k=1		$k=\infty$	
μ	*Ref* [75]	*CFM*	*Ref* [75]	*CFM*	*Ref* [75]	*CFM*
0	8.4813	8.48136	6.5372	6.61797	4.4068	4.40684
1	8.3621	8.36214	6.4452	6.52535	4.3449	4.3449
2	8.2476	8.2477	6.357	6.43622	4.2854	4.28544
3	8.1377	8.13774	6.2721	6.35056	4.2283	4.22831
4	8.03196	8.0319	6.1906	6.28512	4.1733	4.17334
5	7.9301	7.93012	6.112	6.18883	4.1204	4.12042

Table 7 (C–C) FG nanobeam, $L/h = 20$: fundamental nondimensional frequency vs μ for various k comparison with present CFM for TBT

	k=0		k=1		k=∞	
μ	Ref [75]	CFM	Ref [75]	CFM	Ref [75]	CFM
0	12.2201	12.2201	9.4292	9.4292	6.3495	6.34949
1	12.0372	12.0373	9.2878	9.2878	6.2545	6.25447
2	11.862	11.8621	9.1524	9.15237	6.1635	6.16345
3	11.694	11.6941	9.0225	9.02248	6.0762	6.07617
4	11.5327	11.5329	8.8979	8.89785	5.9924	5.99238
5	11.3778	11.3779	8.7781	8.77807	5.9119	5.91185

Table 8 (S–S) FG nanobeam, $L/h = 100$: fundamental nondimensional frequency vs μ for various k comparison with present CFM for TBT

	k=0		k=1		k= ∞	
μ	Ref [75]	CFM	Ref [75]	CFM	Ref [75]	CFM
0	5.4824	5.48243	4.2203	4.22029	2.8486	2.84863
1	5.4797	5.47973	4.2183	4.21821	2.8472	2.84718
2	5.477	5.47703	4.2162	4.21619	2.8458	2.84582
3	5.4743	5.47434	4.2141	4.21406	2.8444	2.84442
4	5.4716	5.47164	4.212	4.21198	2.843	2.84302
5	5.4689	5.46896	4.21	4.20991	2.8416	2.84162

Table 9 (C–S) FG nanobeam, $L/h = 100$: fundamental nondimensional frequency vs μ various k comparison with present CFM for TBT

	k=0		k=1		k=∞	
μ	Ref [75]	CFM	Ref [75]	CFM	Ref [75]	CFM
0	8.5625	8.56262	6.5917	6.67424	4.4491	4.44906
1	8.5576	8.55769	6.5879	6.67041	4.4465	4.44651
2	8.5527	8.55278	6.5841	6.66659	4.444	4.44395
3	8.5478	8.54787	6.5803	6.66277	4.4414	4.4414
4	8.5429	8.54297	6.5766	6.65896	4.4389	4.43886
5	8.538	8.53808	6.5728	6.65516	4.4363	4.43631

(nonlocal softening), and at any fixed μ, they decrease systematically as the grading shifts toward the softer constituent (larger k). The classical boundary hierarchy–$C > C–S > S–S$ holds with preserved mode ordering and no curve crossings; sensitivity to both μ and k increases from the fundamental to higher modes. The cantilever (C–Free) set complements these trends: modes 2–3 follow the same softening-with- μ and soft-grading ordering as the supported cases, whereas the fundamental exhibits a mild, monotonic rise with μ over the reported range an exception confined to this boundary/mode that does not disrupt the overall ordering. Mechanistically, the data reflect three robust effects: nonlocality relaxes effective bending rigidity; softer grading lowers sectional stiffness moments; and stronger end constraints elevate the spectrum by restricting

Table 10 (C–C) FG nanobeam, $L/h = 100$: fundamental nondimensional frequency vs μ for various k comparison with present CFM for TBT

μ	k=0		k=1		$k=\infty$	
	Ref [75]	CFM	Ref [75]	CFM	Ref [75]	CFM
0	12.4214	12.4215	9.5628	9.5628	6.4541	6.45413
1	12.4138	12.4139	9.5569	9.55692	6.4502	6.45016
2	12.4062	12.4063	9.5511	9.55106	6.4462	6.44621
3	12.3986	12.3987	9.5452	9.5452	6.4423	6.44225
4	12.391	12.3911	9.5394	9.53936	6.4383	6.43831
5	12.3834	12.3835	9.5335	9.53352	6.4344	6.43437

Table 11 (S–S) FG nanobeam, $L/h = 10$: fundamental nondimensional frequency vs μ with present CFM for TBT

μ	k=0	k=1	k=3	k=5	k=10	$k=\infty$
0	5.39329	4.44847	4.1021	3.9509	3.68505	2.80231
1	5.14535	4.24387	3.91327	3.76909	3.51558	2.67348
2	4.92873	4.06512	3.74833	3.61027	3.36752	2.56093
3	4.73736	3.90721	3.60262	3.46997	3.23672	2.46149
4	4.56667	3.76638	3.47268	3.34485	3.12006	2.37281
5	4.4132	3.63976	3.35586	3.23236	3.01518	2.29306

Table 12 C–S FG nanobeam, $L/h = 10$: fundamental nondimensional frequency vs μ for present CFM for TBT

μ	k=0	k=1	k=3	k=5	k=10	$k=\infty$
0	8.24263	6.45268	5.74536	5.59582	5.36871	4.2828
1	7.80898	6.11318	5.44369	5.30229	5.08731	4.05748
2	7.43595	5.82119	5.18416	5.04972	4.84511	3.86366
3	7.11083	5.56672	4.95793	4.8295	4.6339	3.69473
4	6.82427	5.34247	4.75852	4.63536	4.44768	3.54584
5	6.56931	5.14294	4.58106	4.46258	4.28194	3.41336

Table 13 (C–C) FG nanobeam, $L/h = 10$: fundamental nondimensional frequency vs μ for present CFM for TBT

μ	k=0	k=1	k=3	k=5	k=10	$k=\infty$
0	11.6518	9.0476	7.97557	7.77391	7.49042	6.05417
1	11.0049	8.54185	7.52963	7.34091	7.07557	5.71807
2	10.4517	8.10985	7.14869	6.97074	6.72052	5.4306
3	9.9719	7.73565	6.81871	6.64987	6.41249	5.18131
4	9.55101	7.40765	6.52947	6.36849	6.14218	4.96262
5	9.17809	7.12315	6.27338	6.11925	5.9026	4.76886

Table 14 (C–Free) FG nanobeam, $L/h = 10$ fundamental nondimensional frequency vs μ for present CFM for TBT

μ	k=0	k=1	k=3	k=5	k=10	$k=\infty$
0	7.75225	5.97233	5.28535	5.18187	5.02517	4.02801
1	7.78411	5.99702	5.30709	5.20307	5.04563	4.04456
2	7.81675	6.02231	5.32935	5.2248	5.06659	4.06152
3	7.8502	6.04822	5.35218	5.24706	5.08808	4.0789
4	7.8845	6.0748	5.37558	5.26989	5.11011	4.09672
5	7.9197	6.10208	5.3996	5.29332	5.13273	4.11501

Table 15 C–C) FG nanobeam, $L/h = 5$ for (EBT), first-mode nondimensional frequency vs μ with present CFM

μ	k=0	k=1	k=3	k=5	k=10	$k=\infty$
0	12.1826	9.36422	8.2678	8.10956	7.87968	6.33
1	9.81212	7.53374	6.63681	6.50846	6.32997	5.09829
2	8.43214	6.47069	5.69421	5.58353	5.43287	4.38127
3	7.50465	5.75711	5.0631	4.96438	4.83171	3.89935
4	6.82722	5.23633	4.60321	4.51328	4.39342	3.54737
5	6.3048	4.83493	4.24912	4.16598	4.05584	3.27592

Table 16 C–C) FG nanobeam, $L/h = 5$ for (EBT): second-mode nondimensional frequency vs μ with present CFM

μ	k=0	k=1	k=3	k=5	k=10	$k=\infty$
0	30.2314	24.2588	20.9307	19.7339	18.1565	15.708
1	18.2357	13.9228	12.1362	11.8872	11.6116	9.47514
2	14.0855	10.7494	9.36248	9.16992	8.96059	7.31868
3	11.8885	9.07095	7.89776	7.73503	7.5596	6.17718
4	10.4766	7.99272	6.95757	6.81406	6.66007	5.44354
5	9.47161	7.2255	6.28889	6.15908	6.02021	4.92137

Table 17 (C–C) FG nanobeam, $L/h = 5$ for (EBT): third-mode nondimensional frequency vs μ with present CFM

μ	k=0	k=1	k=3	k=5	k=10	$k=\infty$
0	31.8978	25.5525	22.0957	21.2345	20.5396	16.5738
1	25.0598	18.9876	16.3466	15.9836	15.4404	13.0183
2	18.6596	14.1323	12.155	11.8834	11.6675	9.69538
3	15.5389	11.7652	10.1143	9.88756	9.70948	8.07387
4	13.601	10.296	8.84877	8.64993	8.49499	7.06697
5	12.2473	9.27003	7.96541	7.78616	7.64721	6.36358

Table 18 (C–S) FG nanobeam, $L/h = 5$ for (EBT): first-mode nondimensional frequency vs μ with present CFM

μ	k=0	k=1	k=3	k=5	k=10	$k=\infty$
0	8.40618	6.53688	5.8207	5.68982	5.48829	4.36778
1	6.91669	5.38106	4.79069	4.68197	4.51543	3.59385
2	6.00893	4.67611	4.16286	4.06792	3.92281	3.12219
3	5.38321	4.18993	3.72997	3.64464	3.51438	2.79707
4	4.9188	3.82896	3.40859	3.33045	3.21125	2.55577
5	4.55667	3.54739	3.15794	3.08543	2.97488	2.36761

Table 19 (C–S) FG nanobeam, $L/h = 5$ for (EBT): second-mode nondimensional frequency vs μ with present CFM

μ	k=0	k=1	k=3	k=5	k=10	$k=\infty$
0	25.9646	19.5454	16.8274	16.3765	15.9841	13.491
1	15.5483	11.8884	10.3885	10.1689	9.91935	8.07878
2	12.1512	9.30469	8.1408	7.96977	7.76851	6.31364
3	10.3151	7.90242	6.91633	6.7712	6.59869	5.35966
4	9.12206	6.98978	6.11839	5.99008	5.83691	4.73974
5	8.2668	6.33508	5.54564	5.42938	5.2903	4.29536

Table 20 (C–S) FG nanobeam, $L/h = 5$ for (EBT): third-mode nondimensional frequency vs μ with present CFM

μ	k=0	k=1	k=3	k=5	k=10	$k=\infty$
0	30.2299	25.5493	22.018	20.5939	18.8944	15.708
1	22.7234	17.2032	14.8234	14.4707	14.1559	11.8069
2	16.9728	12.8912	11.1393	10.8914	10.6712	8.8189
3	14.1403	10.7481	9.29222	9.0869	8.90109	7.34717
4	12.3761	9.41029	8.13797	7.95785	7.7941	6.4305
5	11.1422	8.47375	7.32896	7.16674	7.0187	5.78941

Table 21 (S–S) FG nanobeam, $L/h = 5$ for (EBT), first-mode nondimensional frequency vs μ with present CFM

μ	k=0	k=1	k=3	k=5	k=10	$k=\infty$
0	5.39533	4.44877	4.10893	3.96173	3.69773	2.80339
1	4.56841	3.7662	3.47754	3.35325	3.13043	2.3737
2	4.03315	3.32456	3.06925	2.95971	2.76337	2.09559
3	3.65054	3.00897	2.77759	2.67855	2.50105	1.89681
4	3.35955	2.76898	2.55586	2.46479	2.30162	1.74559
5	3.12862	2.57856	2.37996	2.2952	2.1433	1.62561

Table 22 (S–S) FG nanobeam, $L/h = 5$ for (EBT): second-mode nondimensional frequency vs μ with present CFM

μ	k=0	k=1	k=3	k=5	k=10	$k=\infty$
0	20.6187	15.3172	13.0775	12.8113	12.6791	10.7133
1	12.8388	9.7445	8.47635	8.31318	8.14579	6.67093
2	10.1113	7.78855	6.72573	6.59549	6.44773	5.25372
3	8.60803	6.56966	5.74366	5.63197	5.50033	4.47266
4	7.62269	5.82283	5.09486	4.99552	4.87607	3.96069
5	6.91308	5.28374	4.62553	4.53516	4.42518	3.59198

Table 23 (S–S) FG nanobeam, $L/h = 5$ for (EBT): third-mode nondimensional frequency vs μ via present CFM

μ	k=0	k=1	k=3	k=5	k=10	$k=\infty$
0	30.2314	25.5491	22.0124	20.5474	18.749	15.708
1	20.3152	15.57	13.5798	13.2644	12.9244	10.5556
2	15.2253	11.6864	10.2056	9.96891	9.70603	7.91112
3	12.6952	9.74978	8.51841	8.3236	8.09905	6.5963
4	11.1141	8.53806	7.46161	7.28848	7.09312	5.77481
5	10.0068	7.68876	6.72043	6.56447	6.38789	5.19944

Table 24 (C–Free) FG nanobeam, L/h= 5 for (EBT): first-mode nondimensional frequency vs s μ via present CFM

μ	k=0	k=1	k=3	k=5	k=10	$k=\infty$
0	1.93846	1.49136	1.31921	1.29417	1.25648	1.00721
1	1.97157	1.51673	1.34146	1.31598	1.27774	1.02279
2	2.0083	1.54487	1.36614	1.34018	1.30131	1.04349
3	2.04955	1.57648	1.39386	1.36735	1.32779	1.06493
4	2.09663	1.61254	1.42548	1.39835	1.358	1.08939
5	2.15155	1.65461	1.46236	1.4345	1.39323	1.11793

Table 25 (C–Free) FG nanobeam, $L/h = 5$ for(EBT): second-mode nondimensional frequency vs s μ via present CFM

μ	k=0	k=1	k=3	k=5	k=10	$k=\infty$
0	11.6282	8.90317	7.8051	7.64324	7.44276	6.04187
1	9.25544	7.09211	6.22482	6.10084	5.94204	4.80905
2	7.77016	5.95585	5.23009	5.12686	4.99279	4.03731
3	6.72001	5.1522	4.48215	4.43741	4.32066	3.49165
4	5.9202	4.5401	3.99039	3.91223	3.80861	3.07609
5	5.27722	4.04801	3.55954	3.49002	3.39693	2.742

Table 26 (C–Free) FG nanobeam, $L/h = 5$ for (EBT): third-mode nondimensional frequency vs μ via present CFM

μ	k=0	k=1	k=3	k=5	k=10	$k=\infty$
0	15.1157	12.7317	10.8933	10.0823	9.19131	7.85398
1	14.4208	12.1107	10.3252	9.55737	8.72435	7.49292
2	13.8137	10.8927	9.42112	9.02899	8.32481	7.17747
3	12.4036	9.44091	8.18606	8.0024	7.78917	6.4448
4	11.2779	8.58234	7.43453	7.27242	7.11364	5.86193
5	12.3688	10.3738	8.82314	8.20111	7.51642	6.42673

Table 27 (C–C) FG nanobeam, $L/h = 20$ for (EBT): fundamental nondimensional frequency vs μ via present CFM

μ	k=0	k=1	k=3	k=5	k=10	$k=\infty$
0	12.4143	9.55539	8.46055	8.30064	8.05561	6.45035
1	12.2264	9.41074	8.33236	8.17486	7.93359	6.35274
2	12.0466	9.27227	8.20966	8.05447	7.81679	6.25931
3	11.8743	9.13958	8.09208	7.9391	7.70487	6.16977
4	11.7089	9.01227	7.97927	7.82842	7.59749	6.08386
5	11.5501	8.89	7.87093	7.72212	7.49436	6.00135

Table 28 (C–C) FG nanobeam, $L/h = 20$ for (EBT): second-mode nondimensional frequency vs μ via present CFM

μ	k=0	k=1	k=3	k=5	k=10	$k=\infty$
0	34.101	26.2412	23.2223	22.7823	22.1148	20.0762
1	32.2766	24.8366	21.9779	21.5615	20.9302	16.7707
2	30.7123	23.6324	20.9113	20.515	19.9148	15.9579
3	29.3524	22.5855	19.9842	19.6054	19.0321	15.2513
4	28.1563	21.6648	19.1689	18.8055	18.2559	14.6298
5	27.0938	20.847	18.4448	18.0951	17.4741	14.0777

Table 29 (C–C) FG nanobeam, $L/h = 20$ for (EBT): third-mode nondimensional frequency vs μ via present CFM

μ	k=0	k=1	k=3	k=5	k=10	$k=\infty$
0	66.5327	51.1448	45.2238	44.364	43.0791	34.5476
1	59.4707	45.7423	40.4408	39.6714	38.5249	30.9005
2	54.288	41.754	36.9112	36.2087	35.1636	28.2076
3	50.2634	38.6495	34.1713	33.5208	32.5542	26.1164
4	46.6462	36.1645	31.9661	31.3574	30.4539	24.4329
5	44.343	34.1024	30.2951	29.5681	28.717	23.0402

Table 30 (C–S) FG nanobeam, $L/h = 20$ for (EBT), fundamental nondimensional frequency vs μ via present CFM

μ	k=0	k=1	k=3	k=5	k=10	k=∞
0	8.5558	6.66768	5.95517	5.82176	5.60685	4.44552
1	8.43498	6.57377	5.87142	5.73983	5.52782	4.38275
2	8.31902	6.48363	5.79104	5.66119	5.45197	4.3225
3	8.20764	6.39703	5.7138	5.58563	5.3791	4.26462
4	8.10051	6.31374	5.63952	5.51296	5.30901	4.20896
5	7.99739	6.23357	5.56801	5.443	5.24155	4.15538

kinematics. Given the relative slenderness ($L/h = 20$), EBT captures these behaviors cleanly, yielding smooth, well-ordered, anomaly-free curves. Design note: to raise frequencies, favor stiffer grading (smaller k) and more restrictive supports (especially C–C); to lower them, increase μ, bias grading toward the softer constituent (larger k), or employ less restrictive boundaries, with the cantilever giving the lowest absolute values.

Having established the global behavior across boundary conditions, we now move from the tabulated spectra to a visual summary. Focusing on the fixed–pinned (C–S) configuration as a representative case, the forthcoming figures distill the data into mode-wise curves that highlight how gradation and nonlocality act

Table 31 (C–S) FG nanobeam, L/h= 20 for (EBT): second-mode nondimensional frequency vs μ via present CFM

μ	k=0	k=1	k=3	k=5	k=10	$k=\infty$
0	27.6363	21.3334	18.9208	18.5431	17.9642	14.3596
1	26.2594	20.2714	17.9794	17.6204	17.0698	13.6442
2	25.0695	19.3534	17.1655	16.8226	16.2967	13.0259
3	24.0279	18.5497	16.4528	16.1242	15.6199	12.4847
4	23.1063	17.8385	15.8222	15.5061	15.0211	12.0058
5	22.2835	17.2035	15.259	14.9542	14.4863	11.5783

Table 32 (C–S) FG nanobeam, $L/h = 20$ for (EBT): third-mode nondimensional frequency vs μ via present CFM

μ	k=0	k=1	k=3	k=5	k=10	$k=\infty$
0	57.3589	44.1499	39.0525	38.2937	37.1688	29.8032
1	51.4451	39.7183	35.1386	34.4551	33.4384	26.8056
2	47.2729	36.4	32.2063	31.5794	30.645	24.5626
3	43.8876	33.7966	29.9049	29.3225	28.4532	22.8036
4	41.1413	31.684	28.037	27.4907	26.6746	21.3767
5	38.8556	29.9253	26.4817	25.9656	25.1939	20.189

Table 33 (S–S) FG nanobeam, $L/h = 20$ for (EBT): fundamental nondimensional frequency vs μ via present CFM

μ	k=0	k=1	k=3	k=5	k=10	$k=\infty$
0	5.47773	4.51609	4.17389	4.02516	3.75681	2.84618
1	5.41138	4.46137	4.12328	3.97637	3.71129	2.81171
2	5.34738	4.40858	4.07447	3.92931	3.66738	2.77843
3	5.2856	4.35763	4.02735	3.92483	3.625	2.74635
4	5.22591	4.30841	3.98183	3.83999	3.58406	2.71534
5	5.16819	4.26081	3.93782	3.79756	3.54447	2.68535

Table 34 (S–S) FG nanobeam, $L/h = 20$ for (EBT): second-mode nondimensional frequency vs μ via present CFM

μ	k=0	k=1	k=3	k=5	k=10	$k=\infty$
0	21.8438	16.7876	14.8402	14.5618	14.1468	11.3499
1	20.8396	16.0178	14.1613	13.8953	13.4983	10.8281
2	19.9623	15.345	13.5677	13.3127	12.9315	10.3722
3	19.1872	14.7505	13.043	12.7978	12.4306	9.9695
4	18.4962	14.2201	12.5748	12.3383	11.9837	9.6103
5	17.8743	13.7431	12.1537	11.925	11.5818	9.28733

Table 35 (S–S) FG nanobeam, $L/h = 20$ for (EBT): third-mode nondimensional frequency vs μ with present CFM

μ	k=0	k=1	k=3	k=5	k=10	$k=\infty$
0	48.8999	37.8993	33.6924	32.9754	31.8693	25.408
1	44.2344	34.2887	30.4865	29.8374	28.8338	22.9838
2	40.6916	31.5482	28.0502	27.2169	26.5276	21.143
3	37.883	29.3707	26.1179	25.5613	24.6988	19.6837
4	35.5858	27.5913	24.5368	24.0138	23.2026	18.4901
5	33.6614	26.1005	23.212	22.7171	21.949	17.4902

Table 36 (C–Free) FG nanobeam, $L/h = 20$ for (EBT): fundamental nondimensional frequency vs μ with present CFM

μ	k=0	k=1	k=3	k=5	k=10	$k=\infty$
0	1.95249	1.50293	1.33089	1.30575	1.26714	1.0145
1	1.95458	1.50454	1.33232	1.30715	1.2685	1.01558
2	1.95669	1.50617	1.33375	1.30855	1.26986	1.01668
3	1.9588	1.5078	1.33519	1.30997	1.27124	1.01778
4	1.96094	1.50944	1.33665	1.31139	1.27262	1.01889
5	1.96308	1.51109	1.33811	1.31283	1.27401	1.02

Table 37 (C–Free) FG nanobeam, $L/h = 20$ for (EBT): second-mode nondimensional frequency vs μ with present CFM

μ	k=0	k=1	k=3	k=5	k=10	k=∞
0	12.2008	9.38964	8.31115	8.15384	7.91422	6.33943
1	12.0019	9.23657	8.17564	8.02089	7.78519	6.23609
2	11.8108	9.08948	8.04543	7.89315	7.6612	6.13679
3	11.627	8.94798	7.92017	7.77026	7.54193	6.04127
4	11.4499	8.81172	7.79955	7.65192	7.42707	5.94927
5	11.2792	8.68036	7.68326	7.53783	7.31634	5.86059

Table 38 (C–Free) FG nanobeam, $L/h = 20$ for (EBT): third-mode nondimensional frequency vs μ with present CFM

μ	k=0	k=1	k=3	k=5	k=10	$k=\infty$
0	34.0051	26.1609	23.1395	22.7001	22.0397	17.6687
1	32.2041	24.7754	21.914	21.4978	20.8724	16.733
2	30.6602	23.5877	20.8634	20.4672	19.8718	15.9308
3	29.1342	22.5557	19.9505	19.5717	19.0023	15.2338
4	28.1402	21.6489	19.1484	18.7848	18.2382	14.6214
5	27.0946	20.8445	18.4369	18.0868	17.5607	14.0782

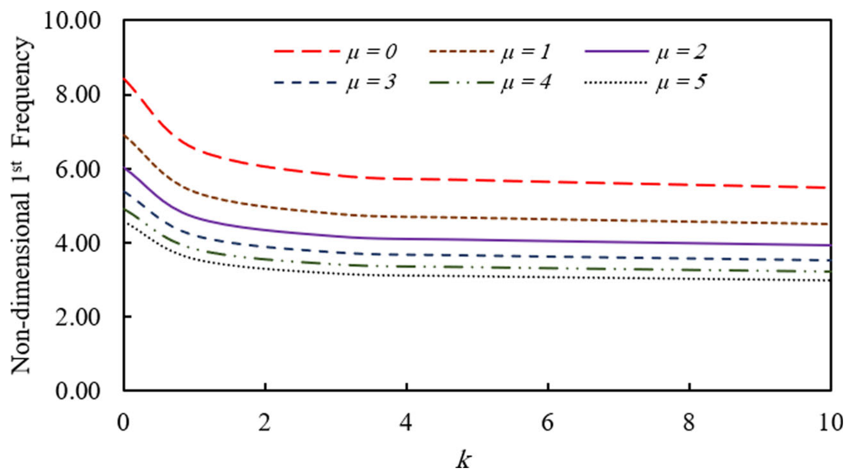

Fig. 2 First nondimensional natural frequency versus gradation index k for an FG nanobeam (Euler–Bernoulli; fixed–pinned, C–S; $L/h = 5$)

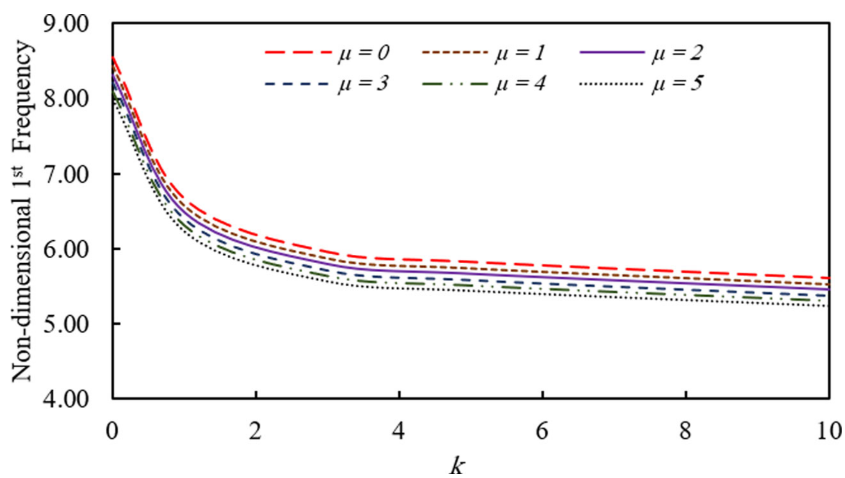

Fig. 3 First nondimensional natural frequency versus gradation index k for an FG nanobeam (Euler–Bernoulli; fixed–pinned; $L/h = 20$; $\mu = 0 - 5$)

across two slenderness ratios, setting the stage for the detailed plots that follow. The tabulated EBT spectra, Figs. 2, 3, 4, 5, 6 and 7, provide a visual representation of the C–S results. Specifically, Fig. 2, 4, and 6 plot the first three modes for $L/h = 5$ using the data in Tables 18–20, while Figs. 3, 5, and 7 plot the corresponding modes for $L/h = 20$ using Tables 30–32.

Figures 3, 4, 5, 6 and 7 plot the nondimensional natural frequencies $\bar{\omega}$ of an FG nanobeam under fixed–pinned (C–S) supports, computed with the present CFM–EBT formulation in the Laplace domain. Each panel shows $\bar{\omega}$ versus the gradation index$k$, with curves for μ =0 − 5, at two slenderness ratios (L/h

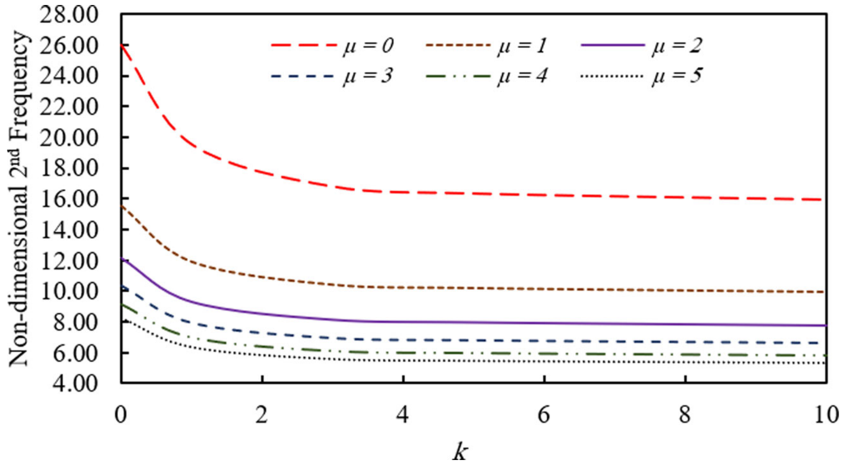

Fig. 4 Second nondimensional natural frequency versus gradation index k for an FG nanobeam (Euler–Bernoulli; fixed–pinned, C–S; $L/h = 5$; $\mu = 0 - 5$)

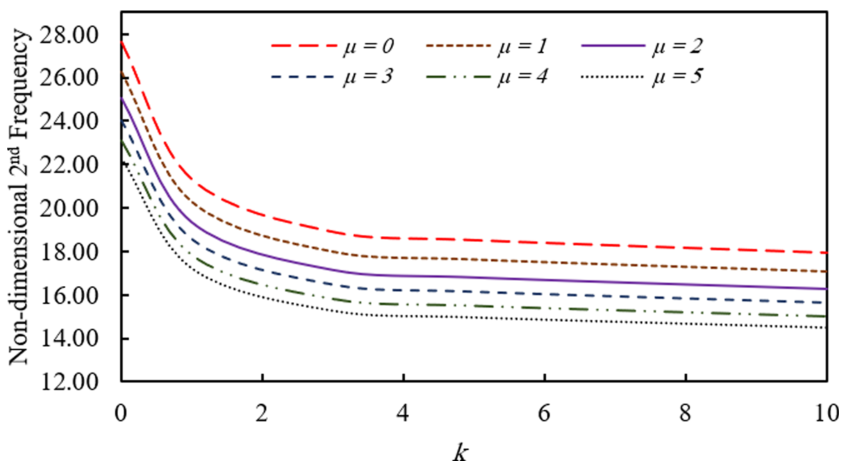

Fig. 5 Second nondimensional natural frequency versus gradation index k for an FG nanobeam (Euler–Bernoulli; fixed–pinned, $L/h = 20\mathrm{L}$, $\mu = 0 - 5$)

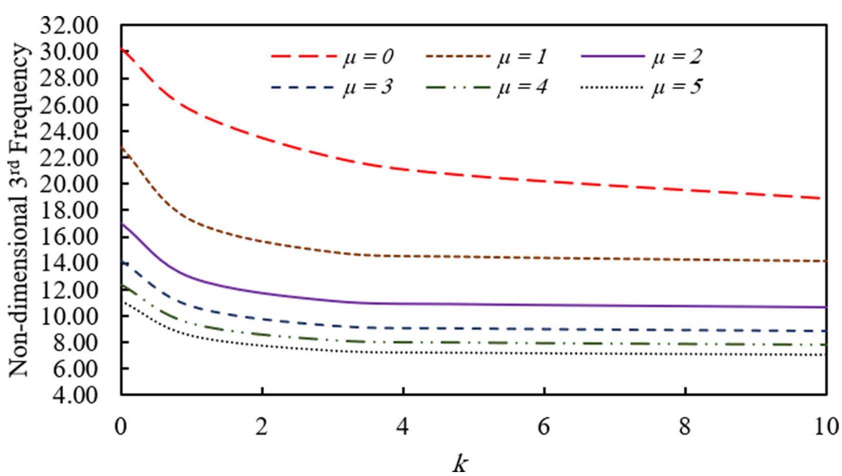

Fig. 6 Third nondimensional natural frequency versus gradation index k for an FG nanobeam (Euler–Bernoulli; fixed–pinned, C–S; $L/h = 5$; $\mu = 0 - 5$)

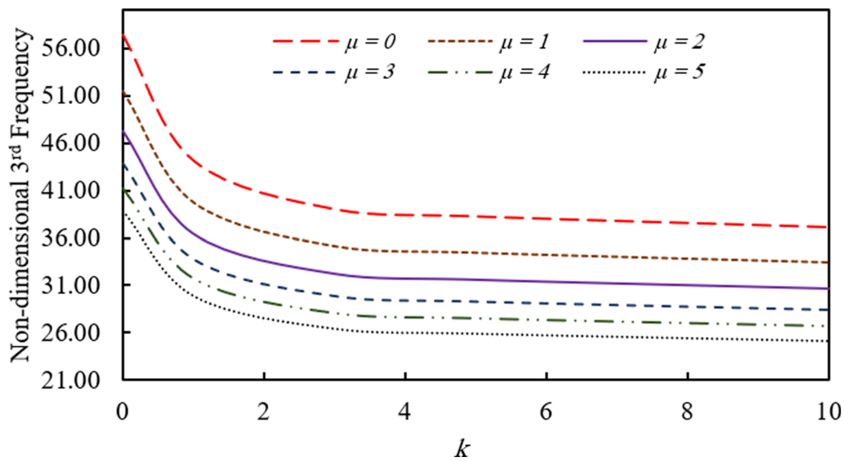

Fig. 7 Third nondimensional natural frequency versus gradation index k for an FG nanobeam (Euler–Bernoulli; fixed–pinned; $L/h = 20$; $\mu = 0 - 5$)

$= 5$ and $L/h = 20$) and for the first three modes. The values are exactly those tabulated in the paper ($L/h =$ 5:Tables 18–20); ($L/h = 20$: Tables 30–32) and are plotted using the normalization defined in Eq. (71).

The plots confirm the expected, smooth trends: for any fixed μ, the frequency decreases monotonically with increasing k (softer grading → lower $\bar{\omega}$), and for any fixed k, increasing μ lowers $\bar{\omega}$ due to nonlocal softening. The $L/h = 20$ set lies systematically above the $L/h = 5$ set under the adopted normalization, while modes 2–3 follow the same patterns as mode 1 with higher magnitudes and slightly stronger sensitivities. Curves exhibit no crossings or anomalies, indicating stable numeric and a faithful visual summary of the table-derived frequency data.

4 Conclusion

This study is intended as a unified formulation and benchmark reference for the free vibration of Eringen-type nonlocal FG nanobeams. Beyond reproducing established trends, it provides a closed-form canonical first-order system for both EBT and TBT within one consistent framework and integrates these operators into a Laplace-domain CFM eigen-solver with determinant-based boundary enforcement. The resulting datasets offer a robust verification base for future developments in refined nonlocal, strain-gradient, surface-energy, or smart-material nanobeam models. The canonical equations are obtained for the first time. Implementation of the CFM in the Laplace domain to the present class of problem is the second novelty of the current paper.

Across the compiled tables, three robust trends emerge:

1. Increasing the nonlocal parameter μ produces monotonic frequency softening.
2. Steering the gradation toward the softer constituent (larger k) further lowers frequencies.
3. The classical boundary hierarchy is preserved (*C–C > C–S > S–S > C–Free*).

As slenderness increases, TBT approaches EBT, and all spectra remain smooth, well-ordered, and free of spurious crossings. A single, interpretable exception appears for the cantilever fundamental, which hardens mildly with μ, while higher cantilever modes follow the general softening trend.

Practically, the tables provide clear tuning rules: to raise frequencies use smaller k and more restrictive supports (especially *C–C*); to lower them increase μ, bias grading toward the softer constituent, or employ less restrictive supports. The methodology is readily extendable to smart and multi-physics nanobeams (e.g., piezoelectric or magneto-electro-elastic FG systems) once physically calibrated nonlocal length scales are available. Overall, the CFM-based formulation delivers accurate, efficient, and reproducible spectra and offers dependable benchmarks for verification and design of nano-engineered beam components. The proposed framework is developed within linear kinematics and the differential form of Eringen's nonlocal elasticity. Extensions to geometric nonlinearity and amplitude-dependent vibration are promising directions for future work building on the present canonical Laplace–CFM formulation. Future extensions may incorporate thermal environments, temperature-dependent FG properties, and thermoelastic pre-stress to broaden applicability to NEMS/MEMS operating conditions.

Although the present manuscript focuses on a classical ceramic–metal FG configuration to establish a clean benchmark baseline, the derived canonical system and the Laplace–CFM solver are not restricted to this material class. The same framework can be directly extended to smart or nano-reinforced FG systems by replacing $E(z)$, $G(z)$, and $\rho(z)$ with the appropriate graded constitutive descriptors and by adopting experimentally calibrated nonlocal length scales.

Author contributions The contributions of Ahmed Mohammad Wasfi Alhasan and Ahmad Reshad Noori to the preparation and writing of this article, including all its sections and scientific content, are equal and carried out with the same level of effort and responsibility.

Funding This research did not receive funding.

Data availability All graphs and data obtained or generated during the investigation appear in the published article.

Declarations

Competing interests The authors declare no competing interests.

References

1. Eringen, A. C. (1983). On differential equations of nonlocal elasticity and solutions of screw dislocation and surface waves (No. RR83SM10).
2. Peddieson, J., Buchanan, G.R., McNitt, R.P.: Application of nonlocal continuum models to nanotechnology. Int. J. Eng. Sci. **41**(3–5), 305–312 (2003)
3. Reddy, J.: Nonlocal theories for bending, buckling and vibration of beams. International journal of engineering science, **45**(2–8), 288–307 (2007)
4. Nazemnezhad, R., Hosseini-Hashemi, S.: Nonlocal nonlinear free vibration of functionally graded nanobeams. Composite Struc. **110**, 192–199 (2014)
5. Esen, I., Abdelrhmaan, A.A., Eltaher, M.A.: Free vibration and buckling stability of fg nanobeams exposed to magnetic and thermal fields. Eng. Comput. **38**(4), 3463–3482 (2022)
6. Ebrahimi, F., Barati, M.R.: A nonlocal higher-order shear deformation beam theory for vibration analysis of size-dependent functionally graded nanobeams. Arab. J. Sci. Eng. **41**(5), 1679–1690 (2016)
7. Pradhan, S.C., Murmu, T.: Application of nonlocal elasticity and DQM in the flapwise bending vibration of a rotating nanocantilever. Phys. E Low Dimens. Syst. Nanostruct. **42**(7), 1944–1949 (2010)
8. Şimşek, M.: Nonlinear free vibration of a functionally graded nanobeam using nonlocal strain gradient theory and a novel Hamiltonian approach. Int. J. Eng. Sci. **105**, 12–27 (2016)
9. Akgöz, B., Civalek, Ö.: Free vibration analysis of axially functionally graded tapered Bernoulli-Euler microbeams based on the modified couple stress theory. Compos. Struct. **98**, 314–322 (2013)
10. Thai, H.T., Vo, T.P.: Bending and free vibration of functionally graded beams using various higher-order shear deformation beam theories. Int. J. Mech. Sci. **62**(1), 57–66 (2012)
11. Thai, H.T., Choi, D.H.: A refined shear deformation theory for free vibration of functionally graded plates on elastic foundation. Compos. Part B Eng. **43**(5), 2335–2347 (2012)
12. Sayyad, A.S., Ghugal, Y.M.: Bending, buckling and free vibration of laminated composite and sandwich beams: a critical review of literature. Compos. Struct. **171**, 486–504 (2017)
13. Tang, Y., Qing, H.: Elastic buckling and free vibration analysis of functionally graded Timoshenko beam with nonlocal strain gradient integral model. Appl. Math. Model. **96**, 657–677 (2021)
14. Aifantis, E.C.: Update on a class of gradient theories. Mech. Mater. **35**(3–6), 259–280 (2003)
15. Reddy, J. N., & Pang, S. D, Nonlocal continuum theories of beams for the analysis of carbon nanotubes. Journal of applied physics, 103(2) (2008)
16. Hosseini, S.A.H., Rahmani, O.: Free vibration of shallow and deep curved FG nanobeam via nonlocal Timoshenko curved beam model. Appl. Phys. A **122**(3), 169 (2016)
17. Huynh, T.A., Luu, A.T., Lee, J.: Bending, buckling and free vibration analyses of functionally graded curved beams with variable curvatures using isogeometric approach. Meccanica **52**(11), 2527–2546 (2017)
18. Gurtin, M.E., Ian Murdoch, A.: A continuum theory of elastic material surfaces. Arch. Ration. Mech. Anal. **57**(4), 291–323 (1975)

19. Hosseini-Hashemi, S., Nazemnezhad, R., Rokni, H.: Nonlocal nonlinear free vibration of nanobeams with surface effects. Eur. J. Mech.-A/Solids **52**, 44–53 (2015)
20. Trabelssi, M., El-Borgi, S., Friswell, M.I.: A high-order FEM formulation for free and forced vibration analysis of a nonlocal nonlinear graded Timoshenko nanobeam based on the weak form quadrature element method. Arch. Appl. Mech. **90**(10), 2133–2156 (2020)
21. Pavić, G.: Numerical study of vibration damping, energy and energy flow in a beam–plate system. J. Sound Vib. **291**(3–5), 902–931 (2006)
22. Ganapathi, M., Merzouki, T., Polit, O.: Vibration study of curved nanobeams based on nonlocal higher-order shear deformation theory using finite element approach. Compos. Struct. **184**, 821–838 (2018)
23. Ghadiri, M., Shafiei, N.: Nonlinear bending vibration of a rotating nanobeam based on nonlocal Eringen's theory using differential quadrature method. Microsyst. Technol. **22**(12), 2853–2867 (2016)
24. Leung, A.Y.T., Mao, S.G.: A symplectic Galerkin method for non-linear vibration of beams and plates. J. Sound Vib. **183**(3), 475–491 (1995)
25. Su, H., Banerjee, J.R.: Development of dynamic stiffness method for free vibration of functionally graded Timoshenko beams. Comput. Struct. **147**, 107–116 (2015)
26. Taima, M.S., El-Sayed, T.A., Farghaly, S.H.: Free vibration analysis of multistepped nonlocal Bernoulli–Euler beams using dynamic stiffness matrix method. J. Vib. Control **27**(7–8), 774–789 (2021)
27. Celebi, K., Yarimpabuc, D., Tutuncu, N.: Free vibration analysis of functionally graded beams using complementary functions method. Arch. Appl. Mech. **88**(5), 729–739 (2018)
28. Yildirim, S.: Free vibration analysis of sandwich beams with functionally-graded-cores by complementary functions method. AIAA J. **58**(12), 5431–5439 (2020)
29. Noori, A.R., Aslan, T.A., Temel, B.: Dynamic analysis of functionally graded porous beams using complementary functions method in the Laplace domain. Compos. Struct. **256**, 113094 (2021)
30. Hosseini, S., Abbaspour, F., Nazari, R.: A new modified Bessel-type radial basis function for meshless methods: utilized in the analysis of free vibration in 2D functionally graded Euler-Bernoulli beams. Int. J. Numer. Model. Electron. Netw. Devices Fields **37**(5), e3287 (2024)
31. Merzouki, T., Houari, M.S.A.: Nonlocal strain gradient theory for free vibration analysis of FG nano-scale beams in thermal environments using an efficient numerical model. J. Vib. Eng. Technol. **12**(7), 8775–8800 (2024)
32. Ehyaei, J., Ebrahimi, F., Salari, E.: Nonlocal vibration analysis of FG nano beams with different boundary conditions. Adv. Nano Res. **4**(2), 085 (2016)
33. Loja, M.A., Rzeszut, K., Barbosa, J.I.: Nonlocal free vibrations of metallic FGM beams. J. Compos. Sci. **6**(5), 125 (2022)
34. Ebrahimi, F., Salari, E.: Nonlocal thermo-mechanical vibration analysis of functionally graded nanobeams in thermal environment. Acta Astronaut. **113**, 29–50 (2015)
35. Ghadiri, M., Jafari, A.: Thermo-mechanical analysis of FG nanobeam with attached tip mass: an exact solution. Appl. Phys. A **122**(12), 1017 (2016)
36. Ebrahimi, F., Salari, E.: Thermal buckling and free vibration analysis of size dependent Timoshenko FG nanobeams in thermal environments. Compos. Struct. **128**, 363–380 (2015)
37. Şimşek, M., Yurtcu, H.H.: Analytical solutions for bending and buckling of functionally graded nanobeams based on the nonlocal Timoshenko beam theory. Compos. Struct. **97**, 378–386 (2013)
38. Hosseini-Hashemi, S., Nahas, I., Fakher, M., Nazemnezhad, R.: Surface effects on free vibration of piezoelectric functionally graded nanobeams using nonlocal elasticity. Acta Mech. **225**(6), 1555–1564 (2014)
39. Wang, C.M., Zhang, Y.Y., He, X.Q.: Vibration of nonlocal Timoshenko beams. Nanotechnology **18**(10), 105401 (2007)
40. Hosseini, S.A., Hamidi, B.A., Behrouzinia, A.: A new model for non-linear vibration of functionally graded porous nanobeam based on non-local curvature and strain gradient tensors. J. Vib. Control **29**(17–18), 4290–4301 (2023)
41. Landau, L. D., Lifshitz, E. M., Kosevich, A. D. M.. Pitaevskii LP Theory of Elasticity (1986)
42. Eringen, A., Wegner, J. Nonlocal continuum field theories. (2003)
43. Wang, Q., Varadan, V.K.: Application of nonlocal elastic beam model to carbon nanotubes. Smart Mater. Struct. **15**(2), 659–666 (2006). https://doi.org/10.1088/0964-1726/15/2/025
44. Timoshenko, S.P.: LXVI. On the correction for shear of the differential equation for transverse vibrations of prismatic bars. Lond. Edinb. Dublin Philos. Mag. J. Sci. **41**(245), 744–746 (1921)
45. Sankar, B.V.: An elasticity solution for functionally graded beams. Compos. Sci. Technol. **61**(5), 689–696 (2001)
46. Aydogdu, M.: A general nonlocal beam theory: its application to nanobeam bending, buckling and vibration. Phys. E Low-Dimens. Syst. Nanostruct. **41**(9), 1651–1655 (2009)
47. Nazmul, I.M., Nahid, S., Indronil, D.: Analytical solutions for vibration of Bi-directional functionally graded nonlocal nanobeams. Results Eng. **18**, 101046 (2023)
48. Bensaid, I.: A refined nonlocal hyperbolic shear deformation beam model for bending and dynamic analysis of nanoscale beams. Adv. Nano Res. **5**(2), 113 (2017)
49. Thai, H.T.: A nonlocal beam theory for bending, buckling, and vibration of nanobeams. Int. J. Eng. Sci. **52**, 56–64 (2012)
50. Noorı, A.R., Aslan, T.A., Temel, B.: Static analysis of FG beams via complementary functions method. Eur. Mech. Sci. **4**(1), 1–6 (2020)
51. Thai, H.T., Park, M., Choi, D.H.: A simple refined theory for bending, buckling, and vibration of thick plates resting on elastic foundation. Int. J. Mech. Sci. **73**, 40–52 (2013)
52. Alshorbagy, A.E., Eltaher, M.A., Mahmoud, F.F.: Static analysis of nanobeams using nonlocal FEM. J. Mech. Sci. Technol. **27**(7), 2035–2041 (2013)
53. Shanab, R.A., Attia, M.A.: Semi-analytical solutions for static and dynamic responses of bi-directional functionally graded nonuniform nanobeams with surface energy effect. Eng. Comput. **38**(3), 2269–2312 (2022)
54. Rasooli, H., Noori, A. R., Temel, B.. Static analysis of functionally graded porous beam-column frames by the complementary functions method. In Structures (Vol. 62, p. 106136). Elsevier (2024, April)

55. Noorı, A.R.: Tamamlayıcı Fonksiyonlar Yöntemi ile Fonksiyonel Derecelenmiş Sandviç Dairesel Plakların Eğilme Analizi. Çukurova Üniversitesi Mühendislik Fakültesi Dergisi **37**(3), 673–684 (2022)
56. Fereidoon, A., Asghardokht Seyedmahalle, M., Mohyeddin, A.: Bending analysis of thin functionally graded plates using generalized differential quadrature method. Arch. Appl. Mech. **81**(11), 1523–1539 (2011)
57. Nejad, M.Z., Hadi, A.: Non-local analysis of free vibration of bi-directional functionally graded Euler–Bernoulli nano-beams. Int. J. Eng. Sci. **105**, 1–11 (2016)
58. Uymaz, B.: Analytical solution of bending, buckling, and vibration of functionally graded nanobeams based on nonlocal elasticity. J. Balkan Sci. Technol. **2**(1), 37–47 (2023)
59. Li, L., Hu, Y.: Buckling analysis of size-dependent nonlinear beams based on a nonlocal strain gradient theory. Int. J. Eng. Sci. **97**, 84–94 (2015)
60. Li, X.F.: A unified approach for analyzing static and dynamic behaviors of functionally graded Timoshenko and Euler–Bernoulli beams. J. Sound Vib. **318**(4–5), 1210–1229 (2008)
61. Calim, F.F.: Free and forced vibration analysis of axially functionally graded Timoshenko beams on two-parameter viscoelastic foundation. Compos. Part B Eng. **103**, 98–112 (2016)
62. Calim, F.F.: Vibration analysis of functionally graded Timoshenko beams on Winkler–Pasternak elastic foundation. Iran. J. Sci. Technol. Trans. Civ. Eng. **44**(3), 901–920 (2020)
63. Mirafzal, A., Fereidoon, A.: Dynamic characteristics of temperature-dependent viscoelastic FG nanobeams subjected to 2D-magnetic field under periodic loading. Appl. Phys. A **123**(4), 247 (2017)
64. Ansari, R., Sahmani, S.: Bending behavior and buckling of nanobeams including surface stress effects corresponding to different beam theories. Int. J. Eng. Sci. **49**(11), 1244–1255 (2011)
65. Akgöz, B., Civalek, Ö.: Strain gradient elasticity and modified couple stress models for buckling analysis of axially loaded micro-scaled beams. Int. J. Eng. Sci. **49**(11), 1268–1280 (2011)
66. Civalek, Ö., Demir, Ç.: Bending analysis of microtubules using nonlocal Euler–Bernoulli beam theory. Appl. Math. Model. **35**(5), 2053–2067 (2011)
67. Akgöz, B., Civalek, Ö.: A size-dependent shear deformation beam model based on the strain gradient elasticity theory. Int. J. Eng. Sci. **70**, 1–14 (2013)
68. Jalaei, M.H., Civalek, Ö: On dynamic instability of magnetically embedded viscoelastic porous FG nanobeam. Int. J. Eng. Sci. **143**, 14–32 (2019)
69. Tounsi, A., Houari, M.S.A., Benyoucef, S., Bedia, E.A.A.: A refined trigonometric shear deformation theory for thermoelastic bending of functionally graded sandwich plates. Aerosp. Sci. Technol. **24**(1), 209–220 (2013)
70. Bourada, M., Kaci, A., Houari, M.S.A., Tounsi, A.: A new simple shear and normal deformations theory for functionally graded beams. Steel Compos. Struct. **18**(2), 409–423 (2015)
71. Al-Basyouni, K.S., Tounsi, A., Mahmoud, S.R.: Size dependent bending and vibration analysis of functionally graded micro beams based on modified couple stress theory and neutral surface position. Compos. Struct. **125**, 621–630 (2015)
72. Alimirzaei, S., Mohammadimehr, M., Tounsi, A.: Nonlinear analysis of viscoelastic micro-composite beam with geometrical imperfection using FEM: MSGT electro-magneto-elastic bending, buckling and vibration solutions. Struct. Eng. Mech. **71**(5), 485–502 (2019)
73. Belabed, Z., Houari, M.S.A., Tounsi, A., Mahmoud, S.R., Bég, O.A.: An efficient and simple higher order shear and normal deformation theory for functionally graded material (FGM) plates. Compos. B Eng. **60**, 274–283 (2014)
74. Aria, A.I., Friswell, M.I.: A nonlocal finite element model for buckling and vibration of functionally graded nanobeams. Compos. Part B Eng. **166**, 233–246 (2019)
75. Yildirim, S., Tutuncu, N.: On the inertio-elastic instability of variable-thickness functionally-graded disks. Mech. Res. Commun. **91**, 1–6 (2018)
76. Yildirim, S., Tutuncu, N.: Radial vibration analysis of heterogeneous and non-uniform disks via complementary functions method. J. Strain Anal. Eng. Des. **53**(5), 332–337 (2018)
77. Yildirim, S., Tutuncu, N.: Axisymmetric plane vibration analysis of polar-anisotropic disks. Compos. Struct. **194**, 509–515 (2018)
78. Calim, F.F.: Transient analysis of axially functionally graded Timoshenko beams with variable cross-section. Compos. Part B Eng. **98**, 472–483 (2016)
79. Calim, F.F.: Dynamic response of curved Timoshenko beams resting on viscoelastic foundation. Struct. Eng. Mech. **59**(4), 761–774 (2016)
80. Celebi, K., Yarimpabuç, D., Keles, I.: A novel approach to thermal and mechanical stresses in a FGM cylinder with exponentially-varying properties. J. Theor. Appl. Mech. **55**(1), 343–351 (2017)
81. Yarımpabuç, D., Eker, M., & Çelebi, K. (2018). Forced Vibration Analysis of Non-Uniform Piezoelectric Rod by the Complementary Functions Method. Karaelmas Science & Engineering Journal/Karaelmas Fen ve Mühendislik Dergisi, 8(2).
82. Zwayen, R. M. R., Noori, A. R., Khatrush, S., & Aslan, T. A. (2025). A New Approach for the Solution of One-Dimensional Consolidation Equation in Saturated Soils Under Various Time-Varying Loads. Arabian Journal for Science and Engineering, 1–18.
83. Aslan, T. A., Noori, A. R., Temel, B., & Özer, A. P. (2025). Vibration analysis of sandwich beams with non-uniform cross-section made of FGP core and FGM faces resting on Winkler elastic foundation. Mechanics Based Design of Structures and Machines, 1–20.
84. Noori, A.R., Temel, B.: On the vibration analysis of laminated composite parabolic arches with variable cross-section of various ply stacking sequences. Mech. Adv. Mater. Struct. **27**(19), 1658–1672 (2020)
85. Alhasan, A.M.W., Noori, A.R.: Static analysis of functionally graded nanobeams based on Euler–Bernoulli and Timoshenko theories via complementary functions method. Mech. Res. Commun. (2025). https://doi.org/10.1016/j.mechrescom.2025.104571
86. Fan, Y.H., She, G.L., Eltaher, M.A.: Nonlinear vibrations of two-directional functionally graded spinning annular plates with variable thickness. Thin-Walled Struct. (2025). https://doi.org/10.1016/j.tws.2025.113627

87. Fan, Y. H., & She, G. L. (2025). Low-velocity impact response of rotating 2D-FGM annular plates with variable thickness. *Communications in Nonlinear Science and Numerical Simulation*, 109373.
88. Zhao, B., She, G.L.: Vibration analysis of graphene reinforced metal foam coupled plates under arbitrary boundary and coupled conditions. Eng. Struct. **343**, 121143 (2025)
89. Ma, Z. S., She, G. L., & Eltaher, M. A. (2025). Nonlinear internal resonance in graphene platelet-reinforced metal foam plates: Straight-side quadrilateral geometry effects. *Thin-Walled Structures*, 114186.